

Fig. 4. Hepatocyte-specific Bcl-xL/Mcl-1-deficient embryos. Offspring from mating *bcl-x<sup>fllox/+</sup> mcl-1<sup>fllox/+</sup> AlbCre* mice and *bcl-x<sup>fllox/fllox</sup> mcl-1<sup>fllox/fllox</sup>* mice were sacrificed on day 18.5 of gestation. Mice were classified into five groups. The *bcl-x<sup>fllox/+</sup> or fllox mcl-1<sup>fllox/+</sup> or fllox* are indicated by Bcl-xL +/+ Mcl-1 +/+; *bcl-x<sup>fllox/+</sup> mcl-1<sup>fllox/+</sup> AlbCre* are indicated by Bcl-xL +/- Mcl-1 +/-; *bcl-x<sup>fllox/fllox</sup> mcl-1<sup>fllox/+</sup> AlbCre* are indicated by Bcl-xL -/- Mcl-1 +/-; *bcl-x<sup>fllox/+</sup> mcl-1<sup>fllox/fllox</sup> AlbCre* are indicated by Bcl-xL +/- Mcl-1 -/-; *bcl-x<sup>fllox/fllox</sup> mcl-1<sup>fllox/fllox</sup> AlbCre* are indicated by Bcl-xL -/- Mcl-1 -/-. The numbers of embryos analyzed were 30 for Bcl-xL +/+ Mcl-1 +/+, 11 for Bcl-xL +/- Mcl-1 +/-, 8 for Bcl-xL -/- Mcl-1 +/-, 9 for Bcl-xL +/- Mcl-1 -/-, and 10 for Bcl-xL -/- Mcl-1 -/-. (A) Gross appearance of embryos. Representative photo for a litter is shown. (B) Body weight. (C) The ratios of liver weight to body weight. \**P* < 0.05 versus Bcl-xL +/+ Mcl-1 +/+; \*\**P* < 0.05 versus Bcl-xL +/+ Mcl-1 +/+ and Bcl-xL +/- Mcl-1 +/- . (D) Hematoxylin-eosin staining of the liver sections. (E) Western blot of whole-liver lysate for albumin expression. (F) Real-time RT-PCR analysis for transferrin expression. The levels were normalized to the group of Bcl-xL +/+ Mcl-1 +/+. \**P* < 0.05 versus Bcl-xL +/+ Mcl-1 +/+; \*\**P* < 0.05 versus Bcl-xL +/+ Mcl-1 +/+ and Bcl-xL +/- Mcl-1 +/- .

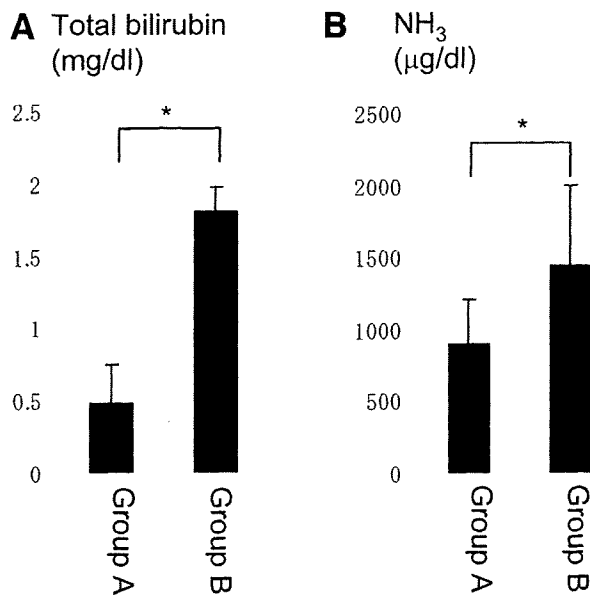


Fig. 5. Plasma biochemistry of hepatocyte-specific Bcl-xL/Mcl-1-deficient neonates 10 hours after birth. Group A (N = 13) was defined as expected survivors including *AlbCre*-negative mice and *bcl-x<sup>fllox/+</sup> mcl-1<sup>fllox/+</sup> AlbCre* mice. Group B (N = 6) was defined as expected nonsurvivors including *bcl-x<sup>fllox/fllox</sup> mcl-1<sup>fllox/+</sup> AlbCre*, *bcl-x<sup>fllox/+</sup> mcl-1<sup>fllox/fllox</sup> AlbCre*, *bcl-x<sup>fllox/fllox</sup> mcl-1<sup>fllox/fllox</sup> AlbCre*. (A) Plasma total bilirubin levels. \**P* < 0.05. (B) Plasma ammonia levels in both groups. \**P* < 0.05.

are in agreement with theirs and further provide evidence that deletion of a single allele for the *mcl-1* gene fails to produce apoptosis phenotypes under physiological conditions, as observed in knockout of the *bcl-x* gene.<sup>13</sup> Mcl-1 heterozygous disrupted mice did not produce apoptosis at least until 16 weeks of age (our unpublished data). It was demonstrated that hepatocyte-specific Mcl-1 knockout mice showed higher levels of liver injury than control mice on anti-Fas antibody injection.<sup>29</sup> However, because mice lacking both *mcl-1* alleles possess preexisting liver injury, it would be difficult to exactly compare liver injury after anti-Fas antibody injection and to conclude whether decreased Mcl-1 expression actually increases the susceptibility to Fas. In the current study, we took advantage of Mcl-1 heterozygous disrupted mice to address this point. They showed significantly higher levels of liver injury after Fas stimulation than wild-type mice, formally proving the significance of Mcl-1 expression under pathological conditions. Furthermore, our data on Mcl-1/Bid-deficient mice implies that the Bid pathway is involved in generating apoptosis found in Mcl-1 knockout mice. Because Bid mediates a variety of cellular stresses in hepatocytes upstream of Mcl-1,<sup>30,31</sup> it will be interesting in future study to determine what stresses generate hepatocyte apoptosis in Mcl-1 knockout mice.

Bcl-xL and Mcl-1 share similar structures and functions.<sup>1</sup> The observations that either deficiency similarly

leads to spontaneous hepatocyte apoptosis imply that they play a non-redundant role in maintaining the integrity of hepatocytes in the adult liver. To further understand the relationship of both molecules, we generated hepatocyte-specific Bcl-xL/Mcl-1 knockout mice. Interestingly, mice lacking single alleles for both genes (*bcl-x<sup>+/-</sup> mcl-1<sup>+/-</sup>*) induced spontaneous hepatocyte apoptosis that could not be distinguished from that found in Bcl-xL or Mcl-1 knockout mice. This indicates that, whereas knockout of a single allele of the *bcl-x* or *mcl-1* gene did not produce apoptosis, knockout of two alleles of any combination among both genes was sufficient to produce hepatocyte apoptosis. This finding suggests that both molecules are not independently but rather interdependently required for ensuring integrity of differentiated hepatocytes.

Bcl-xL/Mcl-1-deficient mice as well as mice only having a single allele of either *bcl-x* or *mcl-1* gene displayed a decreased number of hepatocytes and reduced liver size on day 18.5 of gestation and appeared to develop lethal liver failure within 1 day after birth. Because the liver contains a large number of hematopoietic cells during development (Fig. 4D), it is very difficult to determine the expression levels of Bcl-xL or Mcl-1 specifically in hepatocytes in each knockout mouse. Liver development begins on day 8.5 of gestation in the mouse when the liver primordium is delineated from the endoderm.<sup>32</sup> The albumin promoter, which is active in both hepatoblasts and hepatocytes, shows a 20-fold increase in transcriptional activity from day 9.5 to day 12.5 of gestation. The level of albumin then continues to increase as the liver develops simultaneously with the biliary tree and the hepatic bile duct being formed.<sup>33</sup> Thus, the target genes could probably be successfully deleted during embryogenesis in the *AlbCre* recombination system. The observation that Bcl-xL/Mcl-1-deficient mice developed severer phenotypes than Bcl-xL-deficient or Mcl-1-deficient mice supports the idea that Cre-mediated deletion of the target genes actually took place during embryogenesis in our model. In contrast to the knockout of two alleles, knockout of three alleles and more of the *bcl-x* and *mcl-1* genes induced lethal neonatal hepatic failure. Thus, hepatocyte integrity appeared to be strictly controlled by Bcl-xL and Mcl-1 in a gene dose-dependent manner.

Hepatocyte-specific deficiency of both Bcl-xL and Mcl-1 led to significant reduction of liver volume because of impaired hepatocyte development. However, overall, mice with these phenotypes were capable of developing normally until birth and rapidly developed liver failure and died within 1 day after birth. This finding suggests that differentiated hepatocytes are critically required for maintaining host homeostasis after birth but not during embryogenesis. The placenta

plays an important role in nutritional support and detoxification of the embryo. Our data imply that it could probably compensate for most functions of the liver cells during embryogenesis, whereas the liver would turn to the critical organ that is essential for maintaining host homeostasis after birth. Bcl-xL/Mcl-1 knockout mice provide interesting implications for the difference in the impact of differentiated hepatocytes between embryogenesis and the early neonatal period.

In conclusion, Mcl-1 and Bcl-xL are two major Bcl-2 family proteins inhibiting hepatocyte apoptosis. Together with previous work on traditional knockout mice, our data imply that other members, if any, could not compensate for their functions. Mcl-1 and Bcl-xL cooperatively maintain hepatocyte integrity during liver development and in adult liver homeostasis, and their effects are gene-dose dependent. Recent studies also have established that Mcl-1<sup>5-7</sup> and Bcl-xL<sup>18,34</sup> are frequently overexpressed and confer resistance to apoptosis in hepatocellular carcinoma. Therefore, Mcl-1 and Bcl-xL are important apoptosis antagonists in a variety of pathophysiological conditions of the liver.

**Acknowledgment:** We thank Dr. You-Wen He (Department of Immunology, Duke University Medical Center, Durham, NC) for providing the *mcl-1* floxed mice.

## References

1. Youle RJ, Strasser A. The BCL-2 protein family: opposing activities that mediate cell death. *Nat Rev Mol Cell Biol* 2008;9:47-59.
2. Tsujimoto Y. Cell death regulation by the Bcl-2 protein family in the mitochondria. *J Cell Physiol* 2003;195:158-167.
3. Fischer U, Jänicke RU, Schulze-Osthoff K. Many cuts to ruin: a comprehensive update of caspase substrates. *Cell Death Differ* 2003;10:76-100.
4. Wei MC, Zong WX, Cheng EH, Lindsten T, Panoutsakopoulou V, Ross AJ, et al. Proapoptotic BAX and BAK: a requisite gateway to mitochondrial dysfunction and death. *Science* 2001;292:727-730.
5. Sieghart W, Losert D, Strommer S, Cejka D, Schmid K, Rasoul-Rockenschaub S, et al. Mcl-1 overexpression in hepatocellular carcinoma: a potential target for antisense therapy. *J Hepatol* 2006;44:151-157.
6. Fleischer B, Schulze-Bergkamen H, Schuchmann M, Weber A, Biesterfeld S, Müller M, et al. Mcl-1 is an anti-apoptotic factor for human hepatocellular carcinoma. *Int J Oncol* 2006;28:25-32.
7. Schulze-Bergkamen H, Fleischer B, Schuchmann M, Weber A, Weinmann A, Krammer PH, et al. Suppression of Mcl-1 via RNA interference sensitizes human hepatocellular carcinoma cells towards apoptosis induction. *BMC Cancer* 2006;6:232.
8. Llovet JM, Bruix J. Molecular targeted therapies in hepatocellular carcinoma. *HEPATOLOGY* 2008;48:1312-1327.
9. Liu L, Cao Y, Chen C, Zhang X, McNabola A, Wilkie D, et al. Sorafenib blocks the RAF/MEK/ERK pathway, inhibits tumor angiogenesis, and induces tumor cell apoptosis in hepatocellular carcinoma model PLC/PRF/5. *Cancer Res* 2006;66:11851-11858.
10. Casado M, Mollá B, Roy R, Fernández-Martínez A, Cucarella C, Mayoral R, et al. Protection against Fas-induced liver apoptosis in transgenic mice expressing cyclooxygenase 2 in hepatocytes. *HEPATOLOGY* 2007;45:631-638.
11. Schulze-Bergkamen H, Brenner D, Krueger A, Suess D, Fas SC, Frey CR, et al. Hepatocyte growth factor induces Mcl-1 in primary human hepatocytes and inhibits CD95-mediated apoptosis via Akt. *HEPATOLOGY* 2004;39:645-654.
12. Baskin-Bey ES, Huang W, Ishimura N, Isomoto H, Bronk SF, Braley K, et al. Constitutive androstane receptor (CAR) ligand, TCPOBOP, attenuates Fas-induced murine liver injury by altering Bcl-2 proteins. *HEPATOLOGY* 2006;44:252-262.
13. Takehara T, Tatsumi T, Suzuki T, Rucker EB III, Hennighausen L, Jinushi M, et al. Hepatocyte-specific disruption of Bcl-xL leads to continuous hepatocyte apoptosis and liver fibrotic responses. *Gastroenterology* 2004;127:1189-1197.
14. Dzhagalov I, St John A, He YW. The antiapoptotic protein Mcl-1 is essential for the survival of neutrophils but not macrophages. *Blood* 2007;109:1620-1626.
15. Wagner KU, Claudio E, Rucker EB 3rd, Riedlinger G, Broussard C, Schwartzberg PL, et al. Conditional deletion of the Bcl-x gene from erythroid cells results in hemolytic anemia and profound splenomegaly. *Development* 2000;127:4949-4958.
16. Yin XM, Wang K, Gross A, Zhao Y, Zinkel S, Klocke B, et al. Bid-deficient mice are resistant to Fas-induced hepatocellular apoptosis. *Nature* 1999;400:886-891.
17. Takehara T, Hayashi N, Tatsumi T, Kanto T, Mita E, Sasaki Y, et al. Interleukin 1 $\beta$  protects mice from Fas-mediated hepatocyte apoptosis and death. *Gastroenterology* 1999;117:661-668.
18. Takehara T, Takahashi H. Suppression of Bcl-xL deamidation in human hepatocellular carcinomas. *Cancer Res* 2003;63:3054-3057.
19. Scaffidi C, Fulda S, Srinivasan A, Friesen C, Li F, Tomaselli KJ, et al. Two CD95 (APO-1/Fas) signaling pathways. *EMBO J* 1998;17:1675-1687.
20. Faubion WA, Guicciardi ME, Miyoshi H, Bronk SF, Roberts PJ, Svingen PA, et al. Toxic bile salts induce rodent hepatocyte apoptosis via direct activation of Fas. *J Clin Invest* 1999;103:137-145.
21. Tosh D, Shen CN, Slack JM. Differentiated properties of hepatocytes induced from pancreatic cells. *HEPATOLOGY* 2002;36:534-543.
22. Veis DJ, Sorenson CM, Shutter JR, Korsmeyer SJ. Bcl-2-deficient mice demonstrate fulminant lymphoid apoptosis, polycystic kidneys, and hypopigmented hair. *Cell* 1993;75:229-240.
23. Nakayama K, Nakayama K, Negishi I, Kuida K, Sawa H, Loh DY. Targeted disruption of Bcl-2 alpha beta in mice: occurrence of gray hair, polycystic kidney disease, and lymphocytopenia. *Proc Natl Acad Sci U S A* 1994;91:3700-3704.
24. Print CG, Loveland KL, Gibson L, Meehan T, Stylianou A, Wreford N, et al. Apoptosis regulator bcl-w is essential for spermatogenesis but appears otherwise redundant. *Proc Natl Acad Sci U S A* 1998;95:12424-12431.
25. Ross AJ, Waymire KG, Moss JE, Parlow AF, Skinner MK, Russell LD, et al. Testicular degeneration in Bclw-deficient mice. *Nat Genet* 1998;18:251-256.
26. Hamasaki A, Sendo F, Nakayama K, Ishida N, Negishi I, Nakayama K, et al. Accelerated neutrophil apoptosis in mice lacking A1-a, a subtype of the bcl-2-related A1 gene. *J Exp Med* 1998;188:1985-1992.
27. Motoyama N, Wang F, Roth KA, Sawa H, Nakayama K, Nakayama K, et al. Massive cell death of immature hematopoietic cells and neurons in Bcl-x-deficient mice. *Science* 1995;267:1506-1510.
28. Rinkenberger JL, Horning S, Klocke B, Roth K, Korsmeyer SJ. Mcl-1 deficiency results in peri-implantation embryonic lethality. *Genes Dev* 2000;14:23-27.
29. Vick B, Weber A, Urbanik T, Maass T, Teufel A, Krammer PH, et al. Knock-out of myeloid cell leukemia-1 induces liver damage and increases apoptosis susceptibility of murine hepatocytes. *HEPATOLOGY* 2009;49:627-636.
30. Yin XM. Bid, a BH3-only multi-functional molecule, is at the cross road of life and death. *Gene* 2006;369:7-19.
31. Malhi H, Gores GJ. Cellular and molecular mechanisms of liver injury. *Gastroenterology* 2008;134:1641-1654.
32. Kaestner KH. The making of the liver: developmental competence in foregut endoderm and induction of the hepatogenic program. *Cell Cycle* 2005;4:146-148.
33. Cascio S, Zaret KS. Hepatocyte differentiation initiates during endodermal-mesenchymal interactions prior to liver formation. *Development* 1991;113:217-225.
34. Takehara T, Liu X, Fujimoto J, Friedman SL, Takahashi H. Expression and role of Bcl-xL in human hepatocellular carcinomas. *HEPATOLOGY* 2001;34:55-61.

## Case report

# Two types of drug-resistant hepatitis B viral strains emerging alternately and their susceptibility to combination therapy with entecavir and adefovir

Nao Kurashige<sup>1</sup>, Kazuyoshi Ohkawa<sup>1</sup>, Naoki Hiramatsu<sup>1</sup>, Tsugiko Oze<sup>1</sup>, Takayuki Yakushijin<sup>1</sup>, Kiyoshi Mochizuki<sup>1</sup>, Atsushi Hosui<sup>1</sup>, Takuya Miyagi<sup>1</sup>, Hisashi Ishida<sup>1</sup>, Tomohide Tatsumi<sup>1</sup>, Tatsuya Kanto<sup>1</sup>, Tetsuo Takehara<sup>1</sup> and Norio Hayashi<sup>1\*</sup>

<sup>1</sup>Department of Gastroenterology and Hepatology, Osaka University Graduate School of Medicine, Suita, Osaka, Japan

\*Corresponding author: e-mail: hayashin@gh.med.osaka-u.ac.jp

The most serious problem of nucleoside/nucleotide analogue therapy for hepatitis B virus (HBV) infection is the emergence of drug-resistant mutant virus. Here, we describe a patient with chronic hepatitis B infection with a complex drug-resistant mutant virus during sequential therapy with lamivudine (3TC), entecavir (ETV) and adefovir dipivoxil (ADV). The patient was a 52-year-old male with positive hepatitis B e antigen and high HBV DNA (>7.6 log<sub>10</sub> copies/ml). Initial 3TC monotherapy offered little benefit and 3TC resistance was established by the virus with rtA181T and not rtM204V/I. HBV DNA was reduced slightly by replacement with ETV monotherapy and was followed by virological breakthrough. At that time, rtA181T was undetectable and the virus with rtM204V and rtL180M became predominant. ETV resistance was established by an additional rtS202G

mutation. Efficacy of subsequent combination therapy with ADV and 3TC was limited because of reappearance of the virus with rtA181T, which might confer cross-resistance to 3TC and ADV. Final combination therapy with ETV and ADV reduced HBV DNA to 3.7 log<sub>10</sub> copies/ml for 5 months, which was the most effective therapy for this patient. Thus, two kinds of mutant viruses (rtM204V-related and rtA181T-related) appeared alternately in this patient. Combination therapy with ETV and ADV might have been effective because these drugs share therapeutic roles, that is, ETV affects the rtA181T-related virus and ADV affects the rtM204V-related virus. This is the first report suggesting clinical significance of combination therapy with ETV and ADV for controlling replication of the complex drug-resistant mutant HBV.

## Introduction

Nucleoside/nucleotide analogues have a better therapeutic effect on chronic hepatitis B virus (HBV) infection than previously used drugs. They strongly suppress HBV replication and retard disease progression [1,2]; however, the most serious problem associated with nucleoside/nucleotide analogues is the emergence of drug-resistant viruses through long-term administration. Drug-resistant viruses for nucleoside/nucleotide analogues occur as a result of amino acid substitutions within the reverse transcriptase (RT) domain of the HBV polymerase gene. Lamivudine (3TC) resistance is primarily caused by mutations rtM204V/I and rtL180M, the latter of which is a compensatory substitution [3,4]. Adefovir dipivoxil (ADV) resistance is associated with the mutations rtA181V/T and/or rtN236T [5]. Entecavir (ETV) resistance is established by substitution(s) at rt184, rt202 and/or rt250

in addition to 3TC-resistant substitutions, rtM204V and rtL180M [6].

Recently, the substitution at rt181 has been reported to confer cross-resistance not only to ADV, but also to other nucleoside/nucleotide analogues [7,8]. Some investigators have suggested that 3TC resistance can occur not only with rtM204V/I, but also with rtA181T [9,10]. A more recent report has shown that rtA181V/T is involved in resistance to multiple drugs, including 3TC, ADV and tenofovir disoproxil fumarate, although the degree of drug resistance varies considerably among HBV strains *in vitro* [8].

In this report, we describe a chronic HBV patient who has a complex drug-resistant mutant virus that was identified during sequential therapy with three nucleoside/nucleotide analogues. In this patient, two kinds of mutant viral strains based on the rtM204V and

rtA181T substitutions appeared alternately. We also refer to the clinical usefulness of combination therapy with ETV and ADV for the mutant HBV strain.

### Patient clinical course

The patient was a 52-year-old male who first visited Osaka University Hospital (Osaka, Japan) in September 2004. He had been diagnosed as a chronic HBV carrier 5 years earlier. He was a chronic drinker, with alcohol consumption of approximately 65 g/day. He had also suffered from type-2 diabetes mellitus for >10 years and had undergone insulin therapy for 10 months. The laboratory data at his first visit were alanine aminotransferase (ALT) 68 IU/l (normal level  $\leq 40$  IU/l), aspartate aminotransferase (AST) 75 IU/l (normal level  $\leq 40$  IU/l),  $\gamma$ -glutamyl transpeptidase (GGT) 189 IU/l (normal level  $< 50$  IU/l), fasting plasma glucose (FPG) 239 mg/dl (normal level  $\leq 110$  mg/dl), glycated haemoglobin (HbA1c), 10.3% (normal range 4.3–5.8%) and HBV DNA  $> 7.6 \log_{10}$  copies/ml. Hepatitis B surface antigen (HBsAg) and hepatitis B e antigen (HBeAg) were positive, whereas antibodies against HBsAg (anti-HBs), HBeAg (anti-HBe), hepatitis C virus and HIV were negative. Liver histology showed mild piecemeal necrosis, mild lobular inflammation and mild portal fibrosis; however, steatosis was found in only  $< 5\%$  of the hepatocytes. 3TC (100 mg/day) therapy was commenced in October 2004. Sequencing analysis before therapy revealed no drug-resistance-associated mutations. After starting 3TC therapy, HBV DNA decreased to  $6.5 \log_{10}$  copies/ml in February 2006 and increased again to  $> 7.6 \log_{10}$  copies/ml in April 2006. ALT levels were almost abnormal and on one occasion flared up to 472 IU/l in December 2005 despite cessation of drinking. rtM204V/I was not detected by repeated PCR-enzyme-linked missequence assay [11], but rtA181T was found by sequencing analysis in October 2006. At this point, 3TC was switched to ETV monotherapy (0.5 mg/day). The laboratory data at the beginning of ETV administration were ALT 64 IU/l, AST 78 IU/l, GGT 268 IU/l and HBV DNA  $> 7.6 \log_{10}$  copies/ml. Diabetes mellitus was improved (FPG 123 mg/dl and HbA1c 6.9%) because of a strict diet. During ETV therapy, HBV DNA decreased to  $5.6 \log_{10}$  copies/ml in February 2007, but virological breakthrough was observed in August 2007 (HBV DNA  $6.7 \log_{10}$  copies/ml). As for drug-resistance-associated mutations, rtM204V and rtL180M were detected in September 2007, and rtS202G was detected in January 2008 despite an increasing dose of ETV (1 mg/day). ETV administration was stopped in March 2008 and replaced by combination therapy of 3TC (100 mg/day) with ADV (10 mg/day). The laboratory data at that time were ALT 29 IU/l, AST 49 IU/l, GGT 161 IU/l and HBV DNA

$7.0 \log_{10}$  copies/ml. The combination therapy led to a slight decrease in HBV DNA to  $5.6 \log_{10}$  copies/ml in June 2008. In September 2008, rtA181T was detected again, whereas rtL180M, rtS202G and rtM204V were not detected. From October 2008, a combination therapy with ADV (10 mg/day) and ETV (0.5 mg/day) was carried out. HBV DNA decreased from 5.8 to  $3.7 \log_{10}$  copies/ml for 5 months.

In this patient, ALT fluctuated within the normal to slightly abnormal range ( $\leq 60$  IU/l) during ETV monotherapy and subsequent combination therapy. Improvement of liver function was observed despite poor control of HBV replication and appeared to be greatly attributed to recovery from alcoholic and diabetes mellitus-related liver diseases. Throughout the follow-up period, no side effects from the nucleoside/nucleotide analogues were observed. The clinical course of the patient is summarized in Figure 1.

### Serological and virological assays for HBV

HBsAg, anti-HBs, HBeAg and anti-HBe were determined by chemiluminescent immunoassays. HBV DNA was quantified by a PCR-based method (Amplicor HBV monitor; Roche Diagnostics, Basel, Switzerland). The 3TC-resistant rtM204V/I substitution was examined by PCR-enzyme-linked missequence assay [11]. Nucleotide sequences of the entire RT region were determined by PCR direct sequencing. The primers BF5 (5'-AAGAGACAGTCATCCTCAGG-3', nucleotides 3183–3202) and BR8 (5'-TTGCGTCAGCAAACACTTGG-3', nucleotides 1195–1176) were used for the amplification. The sequencing analyses were done using sera collected in October 2004, October 2006, September 2007, January 2008 and September 2008 (designated as P1 to P5, respectively; Figure 1).

### Results of sequencing analyses

Sequencing data showed that the patient was infected with HBV genotype C according to phylogenetic tree analysis (data not shown). The results of serial sequencing analyses from P1 to P5 are shown in Figure 2. The virus with rtA181T and rtF221Y was detected at P2. By contrast, the virus with rtL180M, rtM204V, rtL229V and rtL269I became predominant at P3. At P4, rtS202G was added, although it occurred incompletely; however, the dominant virus at P5 possessed rtA181T and rtF221Y and was identical to that at P2.

We also compared HBV DNA sequences around rt180 and rt181 obtained at P1–P5 (Figure 3). At P2 and P5, two types of mutations were identified: one was an A670 mutation causing rtA181T and an in-frame stop codon formation at codon 172 of the S gene, and

the other was a C669/A670 double mutation, which resulted in rtA181 but avoided the stop codon formation in the S gene. At P3 and P4, the A667 mutation, which led to rtL180M, was detected.

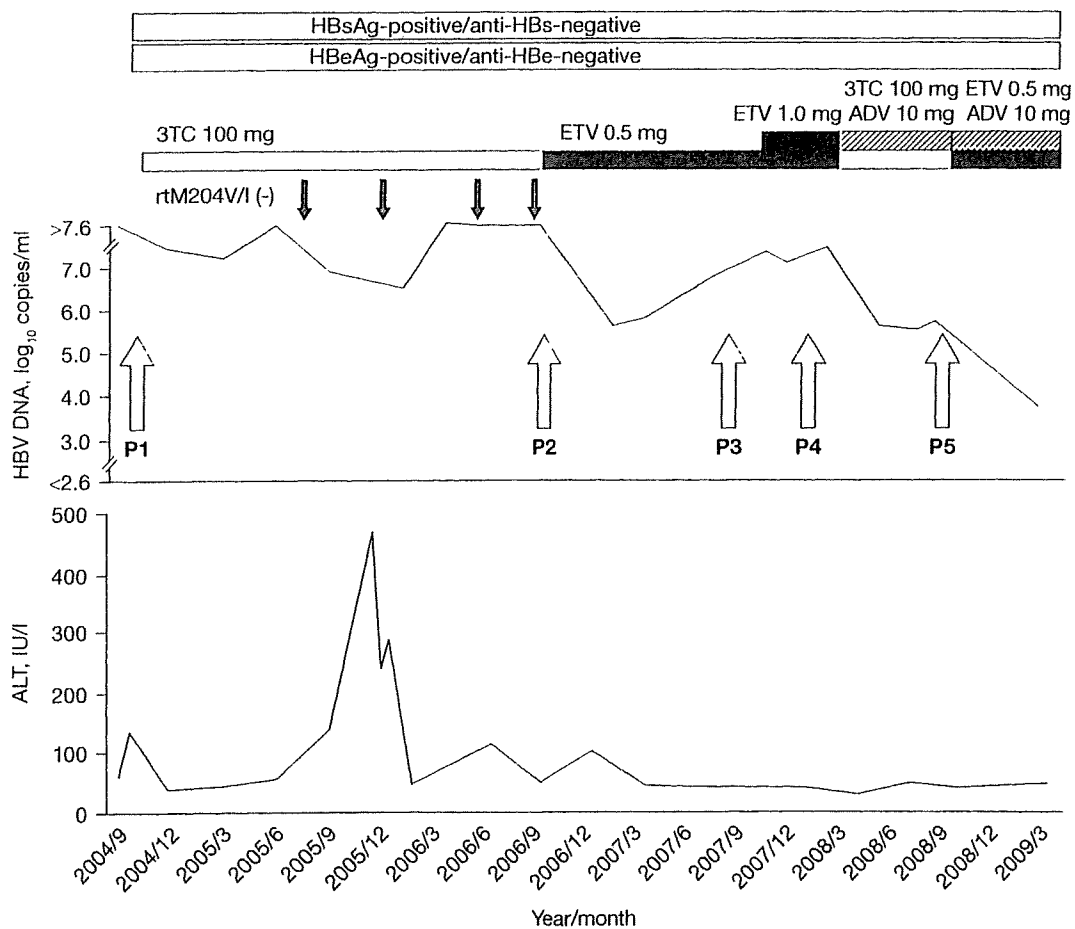
### Discussion

In this paper, we have described a chronic hepatitis B patient with a complex drug-resistant mutant virus. In this patient, initial 3TC monotherapy offered little benefit and virological breakthrough was observed after administration. 3TC resistance was not caused by rtM204V/I but by rtA181T. After 3TC was replaced by ETV, HBV DNA decreased to 5.6 log<sub>10</sub> copies/ml, followed by virological breakthrough for a short period of time. At that time, rtA181T was not detected, and the virus with rtM204V and rtL180M was predominant. This indicates that the virus with rtM204V and

rtL180M might have already coexisted as a minor population before ETV therapy, and that the virus with rtA181T might have been reduced because of its susceptibility to ETV. Indeed, the virus with rtA181V/T has been reported to be sensitive to ETV *in vitro* [8]. The ETV resistance-specific rtS202G was not yet seen at the time of virological breakthrough. It was observed a short time later, resulting in the establishment of ETV resistance, although the reasons for virological breakthrough prior to the detection of the ETV-resistant HBV strain remains to be understood.

Subsequently, combination therapy with ADV and 3TC was done because ADV has been reported to have an effect on ETV resistance [12,13]; however, its efficacy was limited and the virus with rtA181T reappeared. The virus with rtM204V, rtL180M and rtS202G became undetectable. This might be because the virus with rtM204V, rtL180M and rtS202G was susceptible

Figure 1. Clinical course of a patient with a complex drug-resistant mutant HBV during sequential therapy with 3TC, ETV and ADV



Black arrows represent the absence of the rtM204V/I substitution as detected by PCR-enzyme-linked minisequence assay. White arrows represent the serum sampling points (October 2004, October 2006, September 2007, January 2008 and September 2008 designated as P1 to P5, respectively) for sequencing analysis of the hepatitis B virus (HBV) reverse transcriptase region. ADV, adefovir dipivoxil; ALT, alanine aminotransferase; anti-HBe, antibodies against hepatitis B e antigen; anti-HBs, antibodies against hepatitis B surface antigen; ETV, entecavir; HBeAg, hepatitis B e antigen; HBsAg, hepatitis B surface antigen; 3TC, lamivudine.

Figure 2. Amino acid sequences of the RT region of the HBV polymerase gene at serum sampling points P1–P5

	1	50	100
P1	EDWGPCTEHGEHNIRIPRTPARVTGGVFLVDKNPHNTESRLVVDVFSQFSRGSTHVSWPKFVAVPNLQSLTNLLSSNLSWLSLDVSAAFYHIPLHPAAMP		
P2	-----		
P3	-----		
P4	-----		
P5	-----		
	101	150	200
P1	LLVGS SGLPRYVARLSSTSRNIN YQHGTMQDLH DSCSRNLYVSL LLLYKTFGRKLHLYSHPIILGFRKIPMGVGLSPFLLAQFTSAICSVVRRAPPHCLA		
P2	-----		T
P3	-----		M
P4	-----		M
P5	-----		T
	201	250	300
P1	FSYMDDVVLGAKSVQHLESLETSITNFLSLGIHLNPNKTRWGYSLNFMGYVIGSWGTLPOEHIVLKLKQCFRKLVPVNRPIDWKCQRIVGLLGFAAPP		
P2	-----		Y
P3	---V-----		V-----
P4	-G-V-----		V-----
P5	-----		Y
	301		
P1	TQCGYPALMPLYACIQAKQAF TFSPTYKAF LCKQYLHLYPVARQ		
P2	-----		
P3	-----		
P4	-----		
P5	-----		

An amino acid residue identical to that of the top sequence is shown by dashes. The underlined residue indicates the coexistence with the identical residue to the top sequence. Sampling points were at October 2004, October 2006, September 2007, January 2008 and September 2008 (designated as P1 to P5, respectively). HBV, hepatitis B virus; RT, reverse transcriptase.

Figure 3. DNA and amino acid sequences around the positions rt180 and rt181 at serum sampling points P1–P5

				Nucleoside/nucleotide change											
P1	S gene	S	W	L	S										
	Sequence	C	T	C	T	G	G	C	T	C	A	G	T	None	
	Polymerase gene	L		L		A		Q							
				(rt180)				(rt181)							
P2-i	S gene	S													
	Sequence	C	T	C	C	<u>T</u>	<u>G</u>	<u>A</u>	C	T	C	A	G	T	A670
	Polymerase gene	L		L		<u>T</u>		<u>Q</u>							
				(rtA181T)											
P2-ii	S gene	S	S	L	S										
	Sequence	C	T	C	C	T	C	A	C	T	C	A	G	T	C669/A670
	Polymerase gene	L		L		<u>T</u>		<u>Q</u>							
				(rtA181T)											
P3	S gene	S	W	L	S										
	Sequence	C	T	C	A	T	G	G	C	T	C	A	G	T	A667
	Polymerase gene	L		M		A		Q							
				(rtL180M)											

Mutated nucleosides/nucleotides and substituted amino acid residues are underlined. As for nucleoside/nucleotide changes, the nucleoside/nucleotide numbering is according to the representative hepatitis B virus (HBV) genotype C strain (GenBank accession number AB033550) [15], where position 1 is an *EcoRI* recognition site. Sampling points were at October 2004, October 2006, September 2007, January 2008 and September 2008 (designated as P1 to P5, respectively).

to ADV, whereas the virus with rtA181T revealed resistance to 3TC and possibly ADV. Final combination therapy with ETV and ADV resulted in a decrease in HBV DNA to 3.7 log<sub>10</sub> copies/ml for 5 months, which was the most effective therapeutic regimen for this patient. Thus, two kinds of drug-resistant viral strains, the rtA181T-related strain and the rtM204V-related strain, appeared alternately in this patient. It is noteworthy that combination therapy with ETV and ADV was effective against such a complex mutant HBV. This might be because of the sharing of therapeutic roles of these drugs: ETV for the rtA181T-related strain and ADV for the rtM204V-related strain.

rtA181T, which is generally caused by the A670 mutation, results in the in-frame stop codon formation at codon 172 of the S gene. In this patient, the virus with the C669/A670 double mutation, which could produce the surface protein, coexisted with the virus with the A670 mutation alone. A similar virus with the T669/A670 double mutation, which compensates for the defect of surface protein production, has also been reported [7,14].

In summary, we have reported on a complex drug-resistant mutant HBV related to both rtA181T and rtM204V substitutions in a patient with chronic HBV, who received sequential therapy of nucleoside/nucleotide analogues. We also showed for the first time that combination therapy with ETV and ADV might be of clinical significance for controlling replication of complex mutant HBV.

## Disclosure statement

The authors declare no competing interests.

## References

1. Lavanchy D. Hepatitis B virus epidemiology, disease burden, treatment, and current and emerging prevention and control measures. *J Viral Hepat* 2004; 11:97–107.
2. Keeffe EB, Dieterich DT, Han SHB, *et al.* A treatment algorithm for the management of chronic hepatitis B virus infection in the United States: 2008 update. *Clin Gastroenterol Hepatol* 2008; 6:1315–1341.
3. Allen MI, Deslauriers M, Andrews CW, *et al.* Identification and characterization of mutations in hepatitis B virus resistant to lamivudine. *Hepatology* 1998; 27:1670–1677.
4. Liaw YF, Chien RN, Yeh CT, Tsai SL, Chu CM. Acute exacerbation and hepatitis B virus clearance after emergence of YMDD motif mutation during lamivudine therapy. *Hepatology* 1999; 30:567–572.
5. Hadziyannis SJ, Tassopoulos NC, Heathcote EJ, *et al.* Long-term therapy with adefovir dipivoxil for HBeAg-negative chronic hepatitis B for up to 5 years. *Gastroenterology* 2006; 131:1743–1751.
6. Tenney DJ, Rose RE, Baldick CJ, *et al.* Two-year assessment of entecavir resistance in lamivudine-refractory hepatitis B virus patients reveals different clinical outcomes depending on the resistance substitutions present. *Antimicrob Agents Chemother* 2007; 51:902–911.
7. Yatsuji H, Noguchi C, Hiraga N, *et al.* Emergence of a novel lamivudine-resistant hepatitis B virus variant with a substitution outside the YMDD motif. *Antimicrob Agents Chemother* 2006; 50:3867–3874.
8. Villet S, Pichoud C, Billioud G, *et al.* Impact of hepatitis B virus rtA181V/T mutants on hepatitis B treatment failure. *J Hepatol* 2008; 48:747–755.
9. Yeh CT, Chien RN, Chu CM, *et al.* Clearance of the original hepatitis B virus YMDD-motif mutants with emergence of distinct lamivudine-resistant mutants during prolonged lamivudine therapy. *Hepatology* 2000; 31:1318–1326.
10. Pai SB, Bozdayı AM, Pai RB, *et al.* Emergence of a novel mutation in the FLLA region of hepatitis B virus during lamivudine therapy. *Antimicrob Agents Chemother* 2005; 49:2618–2624.
11. Kobayashi S, Ide T, Sata M. Detection of YMDD motif mutations in some lamivudine-untreated asymptomatic hepatitis B virus carriers. *J Hepatol* 2001; 34:584–586.
12. Villet S, Ollivet A, Pichoud C, *et al.* Stepwise process for the development of entecavir resistance in a chronic hepatitis B virus infected patient. *J Hepatol* 2007; 46:531–538.
13. Yatsuji H, Hiraga N, Mori N, *et al.* Successful treatment of an entecavir-resistant hepatitis B virus variant. *J Med Virol* 2007; 79:1811–1817.
14. Yatsuji H, Suzuki F, Sezaki H, *et al.* Low risk of adefovir resistance in lamivudine-resistant chronic hepatitis B patients treated with adefovir plus lamivudine combination therapy: two-year follow-up. *J Hepatol* 2008; 48:923–931.
15. Okamoto H, Tsuda F, Sakugawa H, *et al.* Typing hepatitis B virus by homology in nucleotide sequence: comparison of surface antigen subtypes. *J Gen Virol* 1988; 69:2575–2583.

Accepted for publication 24 May 2009



## Anticancer Chemotherapy Inhibits MHC Class I–Related Chain A Ectodomain Shedding by Downregulating ADAM10 Expression in Hepatocellular Carcinoma

Keisuke Kohga, Tetsuo Takehara, Tomohide Tatsumi, Takuya Miyagi, Hisashi Ishida, Kazuyoshi Ohkawa, Tatsuya Kanto, Naoki Hiramatsu, and Norio Hayashi

Department of Gastroenterology and Hepatology, Osaka University Graduate School of Medicine, Osaka, Japan

### Abstract

MHC class I–related chain A (MICA) is a ligand for the NKG2D-activating immunoreceptor that mediates activation of natural killer (NK) cells. The ectodomain of MICA is shed from tumor cells, which may be an important means of evading antitumor immunity. We previously reported that patients with hepatocellular carcinoma (HCC) display high levels of soluble MICA in circulation, which could be downregulated by chemotherapy. The present study shows that anti-HCC drugs suppress MICA ectodomain shedding by inhibiting expression of a disintegrin and metalloproteinase 10 (ADAM10). Both ADAM10 and CD44, a typical substrate of the ADAM10 protease, were expressed in human HCC tissues and HCC cells but not in normal liver tissues or cultured hepatocytes. Small interfering RNA–mediated knockdown experiments revealed that ADAM10 is a critical sheddase for both MICA and CD44 in HCC cells. Of interest is the finding that epirubicin clearly downregulated ADAM10 expression and MICA shedding in HCC cells; its suppressive effect on MICA shedding was abolished in ADAM10-depleted cells. Epirubicin treatment also enhanced the NKG2D-mediated NK sensitivity of HCC cells. Patients with HCC had significantly higher levels of serum-soluble CD44, which correlated well with serum-soluble MICA levels, thus suggesting a close link between ADAM10 activity and MICA shedding in these patients. Soluble MICA and CD44 levels were downregulated with a significant correlation in patients treated by transarterial chemoembolization using epirubicin. In conclusion, anticancer drugs can modulate expression of ADAM10, which is critically involved in MICA ectodomain shedding. Epirubicin therapy may have a previously unrecognized effect on antitumor immunity in HCC patients. [Cancer Res 2009;69(20):8050–7]

### Introduction

Hepatocellular carcinoma (HCC) is one of the leading causes of cancer deaths worldwide. Chronic liver disease caused by hepatitis virus infection and nonalcoholic steatohepatitis leads to a predisposition for HCC, with liver cirrhosis, in particular, being considered a premalignant condition (1, 2). With regard to

treatment, surgical resection or percutaneous techniques such as ethanol injection and radiofrequency ablation are considered to be choices for curable treatment of localized HCC, whereas transcatheter arterial chemoembolization (TACE) is a well-established technique for more advanced HCC (3). The liver contains a large compartment of innate immune cells [natural killer (NK) cells and natural killer T cells] and acquired immune cells (T cells; refs. 4, 5), but the activation of these immune cells after HCC treatments remains unclear. If such treatments can efficiently activate abundant immune cells in the liver, this could lead to the establishment of attractive new strategies for HCC treatment.

MHC class I–related chain A and B (MICA and MICB) are ligands for NKG2D expressed on a variety of immune cells (6). In contrast to classic MHC class I molecules, MICA/B are rarely expressed on normal cells but frequently on tumor cells (7–10). The engagement of MICA/B and NKG2D strongly activates NK cells and costimulates T cells, enhancing their cytolytic activity and cytokine production (11). Thus, the MICA/B–NKG2D pathway is an important mechanism by which the host immune system recognizes and kills transformed cells (12). In addition to those membrane-bound forms, MICA/B molecules are also cleaved proteolytically from tumor cells and appear as soluble forms in sera of patients with malignancy (13–15). Soluble MICA/B in circulation downregulates NKG2D expression and disturbs NKG2D-mediated antitumor immunity (9, 10, 13). We previously reported that soluble MICA could be detected in sera of HCC patients (16) and that TACE treatment reduces the levels of soluble MICA and thereby upregulates the expression of NKG2D (17). Thus, cancer therapy may have a beneficial effect on NKG2D-mediated immune responses.

The release of soluble MICA/B from tumor cells is impaired by metalloproteinase inhibitors, suggesting the involvement of members of the metzincin superfamily, such as ADAM proteins (14, 18). In addition, ERp5, related to protein disulfide isomerase, is required for the MICA shedding as it reduces disulfide bond of the  $\alpha 3$  domain of MICA (19). Although it may not be a direct protease for MICA, it may enable proteolytic cleavage through conformational change. Recently, it was reported that MICA shedding of 293T fibroblast cells and HeLa cervical cancer cells was inhibited by silencing of the ADAM10 and ADAM17 proteases (20). This suggests that ADAM family proteins may be a therapeutic target for enhancing antitumor immunity, but how to therapeutically modulate these proteins is still not clear. Furthermore, it remains to be determined whether ADAMs can regulate MICA shedding in a clinical setting.

In the present study, we showed that ADAM10, but not ADAM17, was critically required for MICA shedding in human HCC cells. Of importance is the discovery that epirubicin, a widely used anti-HCC drug, was capable of downregulating ADAM10 expression and

Note: Supplementary data for this article are available at Cancer Research Online (<http://cancerres.aacrjournals.org/>).

K. Kohga, T. Takehara, and T. Tatsumi contributed equally to this work.

Requests for reprints: Norio Hayashi, Department of Gastroenterology and Hepatology, Osaka University Graduate School of Medicine, 2-2 Yamadaoka, Suita, Osaka 565-0871, Japan. Phone: 81-6-6879-3621; Fax: 81-6-6879-3629; E-mail: hayashin@gh.med.osaka-u.ac.jp.

©2009 American Association for Cancer Research.

doi:10.1158/0008-5472.CAN-09-0789

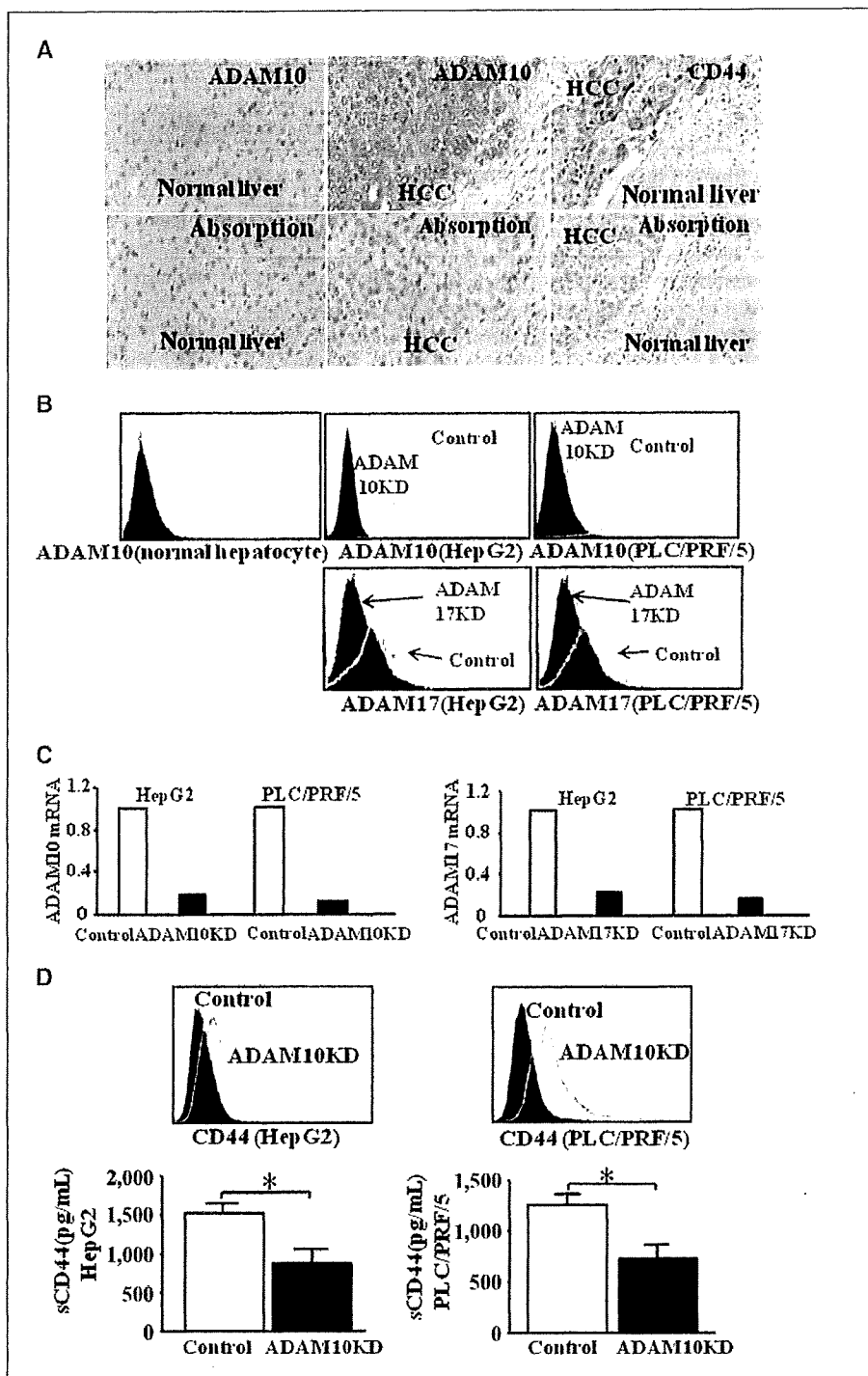
activity in HCC cells; it can thus inhibit MICA shedding and enhance NK sensitivity. ADAM10 was immunohistochemically detected in HCC tissues and a correlation was observed between soluble MICA levels and ADAM10 activity determined by soluble CD44 levels in HCC patients. The present study sheds light on previously unrecognized effects of an anticancer drug on modulating ADAM family proteins and MICA shedding and thus

suggests a promising aspect for chemioimmunotherapy against human HCC.

**Materials and Methods**

**Liver tissues and immunohistochemistry.** Human HCC tissues (*n* = 8) and normal liver tissues (*n* = 2) obtained at surgical resection were used. Informed consent, under an institutional review board-approved protocol,

**Figure 1.** Expression of ADAM10 and CD44 in human HCC tissues and ADAM10 or ADAM17 knockdown in human HCC cells. **A**, immunohistochemical detection of ADAM10 and CD44 in human HCC tissues (*n* = 8) and normal liver tissues (*n* = 2). Liver sections were stained with the corresponding antibodies (top panels). Both primary antibodies were incubated with recombinant CD44 and ADAM10 proteins and then applied to liver sections in parallel as the absorption test (bottom panels). Representative images are shown. **B** and **C**, expression of ADAM10 or ADAM17 in human primary hepatocyte and HCC cell lines (HepG2 and PLC/PRF/5). Cells were treated with ADAM10 siRNA, ADAM17 siRNA, or control siRNA, and subjected to analysis of ADAM10 or ADAM17 expression by flow cytometry (**B**) or real-time RT-PCR (**C**). Histograms, anti-ADAM10 or anti-ADAM17 staining of ADAM10 or ADAM17 siRNA-treated cells (ADAM10KD or ADAM17KD, black dotted line) and control siRNA-treated cells (Control, gray line), respectively. Closed histograms, control IgG staining. **D**, the expression of membrane-bound CD44 on HCC cells treated with ADAM10 siRNA (ADAM10KD, black line) or control siRNA (Control, gray line) was evaluated by flow cytometry (top panels). Closed histograms, control IgG staining. Soluble CD44 (sCD44) production from HCC cells treated with ADAM10 siRNA or control siRNA were evaluated by specific ELISA (bottom panels). \*, *P* < 0.05.



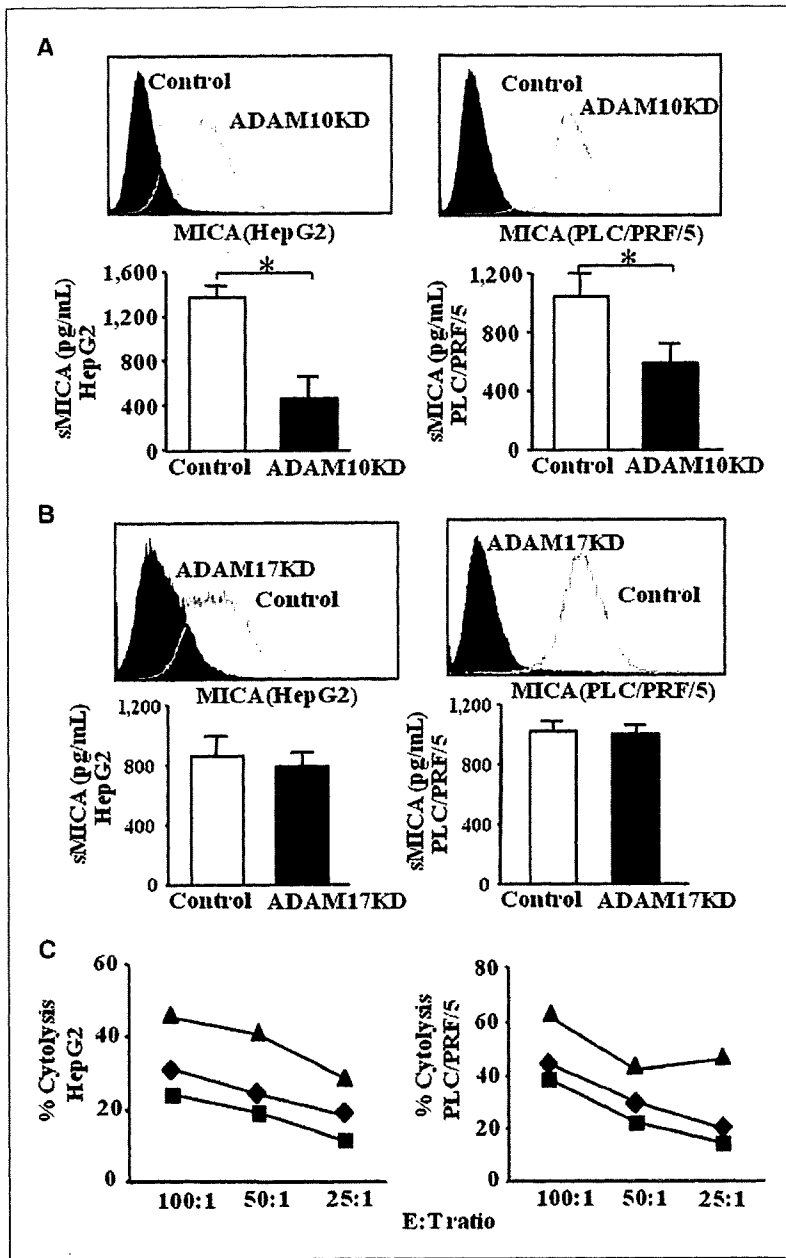


**Figure 2.** Expression of MICA in ADAM10 or ADAM17 knockdown HCC cells and NK sensitivity in ADAM10 knockdown HCC cells. *A* and *B*, the expression of membrane-bound MICA on HCC cells treated with ADAM10 siRNA (*ADAM10KD*, black line; *A*), ADAM17 siRNA (*ADAM17KD*, black line; *B*), or control siRNA (*Control*, gray line) was evaluated by flow cytometry (top panels). Closed histograms, control IgG staining. Soluble MICA (sMICA) production from HCC cells treated with ADAM10 siRNA (*A*), ADAM17 siRNA (*B*), or control siRNA were evaluated by specific ELISA (bottom panels). \*,  $P < 0.05$ . *C*, HCC cells treated with ADAM10 siRNA or control siRNA were subjected to  $^{51}\text{Cr}$ -release assay against NK cells. Cytolytic activity of NK cells against control HCC cells (■) or ADAM10 knockdown HCC cells without (▲) or with blocking antibody of MICA/B (6D4; ◆). Representative results are shown. Similar results were obtained from three independent experiments.

was obtained from all patients before sample acquisition. Liver sections were subjected to immunohistochemical staining using the ABC procedure (Vector Laboratories, Burlingame, CA). The primary antibodies used were anti-ADAM10 and anti-CD44 (R&D Systems). To confirm the specificity of the staining, primary antibodies were incubated with recombinant CD44 or ADAM10 protein (R&D Systems, Minneapolis, MN) for 3 h and then applied onto liver sections in parallel with staining of the primary antibodies as the absorption test.

**HCC cell lines.** Human HCC cell lines HepG2 and PLC/PRF/5 were purchased from the American Type Culture Collection and were cultured with DMEM supplemented with 10% fetal bovine serum (GIBCO/Life Technologies, Grand Island, NY) in a humidified incubator at 5% CO<sub>2</sub> and 37°C.

**RNA silencing.** The small interfering RNA (siRNA) method was used to knockdown ADAM10 and ADAM17. Stealth RNAi oligonucleotide targeting ADAM10 or ADAM17 and scrambled oligonucleotides as a

control were purchased from Invitrogen (Carlsbad, CA). Cells were transfected by RNAi Max transfection reagent (Invitrogen) with 50 nmol/L siRNA. At 24 h posttransfection, the cells were analyzed for specific depletion of the mRNAs of ADAM10 and ADAM17 by real-time reverse transcription-PCR (RT-PCR; Applied Biosystems, Foster City, CA). The following siRNAs were used: ADAM10, 5'-AUAUCUGGGCAAUCACAGCUUCUCG-3'; scramble control, 5'-AUACUUGGUCAACGCACUUCGAUGG-3'; ADAM17, 5'-UGAACAAAGCUCUUCAGGUGGUUCUC-3'; scramble control, 5'-UGAUUAGAACUCUCGACUGGUGUC-3'.

**ELISA.** The supernatants of cultured cells were harvested at 24 h after transfection with siRNA as well as sera from HCC patients ( $n = 97$ ) and age-matched healthy volunteers ( $n = 32$ ) were subjected to analysis of soluble MICA and soluble CD44 levels. Informed consent, under an institutional review board-approved protocol, was obtained from all patients before sample acquisition. The levels of soluble MICA and soluble CD44 were

determined by DuoSet MICA eELISA kit (R&D Systems) and soluble CD44 ELISA (Abcam, Cambridge, MA), respectively.

**Flow cytometry.** For the detection of membrane-bound MICA and CD44, cells were incubated with an anti-MICA-specific antibody (2C10, Santa Cruz Biotechnology, Santa Cruz, CA) or anti-CD44 antibody (R&D Systems) and stained with phycoerythrin (PE)-goat anti-mouse immunoglobulin (Beckman Coulter) as a secondary reagent and then subjected to flow cytometric analysis. For the detection of ADAM10 or ADAM17, cells were fixed and permeabilized with Cytofix/Cytoperm (BD Biosciences, San Jose, CA) and stained with PE-conjugated anti-ADAM10 or anti-ADAM17 antibody (R&D Systems). Flow cytometric analysis was performed using a FACScan flow cytometer (Becton Dickinson).

**Plasmid construction of pMyc-MICA.** MICA full coding cDNA was isolated from Huh7, human HCC cells, using a conventional RT-PCR method (Supplementary Fig. S1, DDBJ/EMBL/Genbank accession number AB506764) and inserted into the *HindIII-XbaI* site of pcDNA3 (Invitrogen). A C-myc tag was placed between the leader peptide and the  $\alpha 1$  domain of MICA by site-specific mutagenesis using a QuikChange site-directed mutagenesis kit (Stratagene, La Jolla, CA) referred to as pMyc-MICA. Cells were transfected with pMyc-MICA using a Lipofectamine LTX reagent (Invitrogen). The green fluorescent protein (GFP)-expressing vector (pEGFP-C1, Clontech, Mountain View, CA) was cotransfected to evaluate the transfection efficiency.

**Immunoprecipitation.** Cells or tissues were homogenized in lysis buffer containing 1% NP40, 0.5% sodium deoxycholate, 0.1% SDS, 50  $\mu\text{g}/\text{mL}$  aprotinin, 100  $\mu\text{g}/\text{mL}$  phenylmethylsulfonyl fluoride, 1 mmol/L sodium orthovanadate, 50 mmol/L sodium fluoride, and PBS. To the cell supernatants, 0.5% NP40 and a cocktail of protease inhibitors were added. The protein contents of the samples were determined by BCA protein assay kit (Pierce, Rockford, IL). Immunoprecipitation with anti-c-Myc beads was performed for 1 h at 4°C. Immunocomplexes were eluted by a c-Myc-tagged peptide solution (MBL, Woburn, MA). The samples after immunoprecipitation were treated with 250 mU of N-glycosidase F (Roche, Mannheim, Germany) for 3 h at 37°C.

**Western blotting.** The total cellular protein was electrophoretically separated using SDS-12% polyacrylamide gels and transferred onto polyvinylidene difluoride membrane. The membrane was blocked in TBS-Tween containing 5% skim milk for 1 h and then probed with anti-Myc mouse monoclonal antibody (Cell Signaling Technology, Danvers, MA) at 4°C overnight. Horseradish peroxidase-conjugated anti-rabbit antibody and SuperSignal West Pico System (Pierce) were used for the detection of blots.

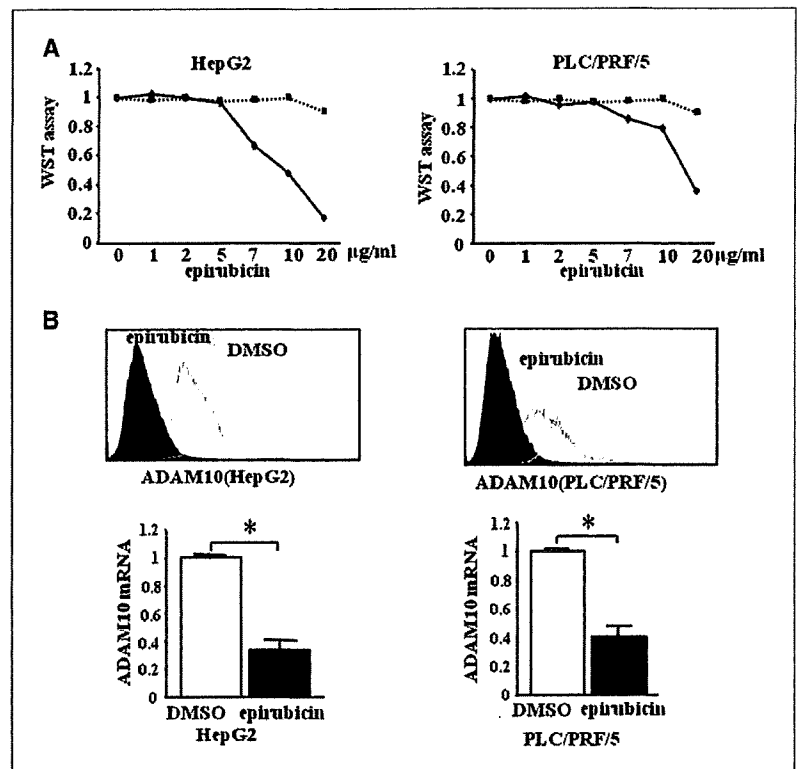
**Real-time RT-PCR.** Total RNA was isolated using RNeasy Mini Kit (Qiagen K.K., Tokyo, Japan) and was reverse transcribed using SuperScript III First-Strand Synthesis System (Invitrogen). The mRNA levels were evaluated using ABI PRISM 7900 Sequence Detection System (Applied Biosystems). Ready-to-use assays (Applied Biosystems) were used for the quantification of ADAM10 (Hs00153853\_m1), ADAM17 (Hs00234221\_m1), MICA (Hs00792195\_m1),  $\beta$ -actin (Hs99999903\_m1), and CD44 (Hs00174139\_m1) mRNAs according to the manufacturer's instructions. The thermal cycling conditions for all genes were 2 min at 50°C and 10 min at 95°C, followed by 40 cycles at 95°C for 15 s and 60°C for 1 min.  $\beta$ -Actin mRNA from each sample was quantified as an endogenous control of internal RNA.

**WST-8 assay.** HepG2 and PLC/PRF/5 cells were treated with different concentrations of epirubicin for 24 h. Cell growth of epirubicin-treated HCC cells was determined by WST-8 assay (Nacalai Tesque, Kyoto, Japan) as previously described (21).

**NK cell analysis.** NK cells were isolated from human peripheral blood mononuclear cells by magnetic cell sorting using CD56 MicroBeads (Miltenyl Biotech, Auburn, CA) as previously described (16). The cytolytic ability of NK cells was assessed by 4-h  $^{51}\text{Cr}$ -releasing assay with or without MICA/B-blocking antibody (6D4; ref. 7), which binds to the  $\alpha 1$  and  $\alpha 2$  domains of MICA and MICB. 6D4 was a generous gift from Drs. Veronika Groh and Thomas Spies (Fred Hutchinson Cancer Research Center, Seattle, WA).

**Statistics.** All values were expressed as the mean and SD. The statistical significance of differences between the groups was determined by applying Student's *t* test or two-sample *t* test with Welch correction after each group

**Figure 3.** Expression of ADAM10 in epirubicin-treated HCC cells. **A**, the cytotoxicity of epirubicin to human HCC cells was evaluated by WST-8 assay. Cells were treated with different doses of epirubicin (solid lines) or vehicle (DMSO; dotted lines) for 24 h, and the viability of the cells was evaluated by the WST-8 assay. **B**, ADAM10 expression of epirubicin-treated HCC cells. Cells were treated with a nontoxic dose of 1  $\mu\text{g}/\text{mL}$  epirubicin (black lines) or vehicle (DMSO, gray lines) for 24 h and their ADAM10 expression was evaluated by flow cytometry (top panels). Closed histograms, control IgG staining. Total RNA was extracted at 24 h of epirubicin treatment and mRNA levels of ADAM10 were evaluated by real-time RT-PCR (bottom panels). \*,  $P < 0.05$ .



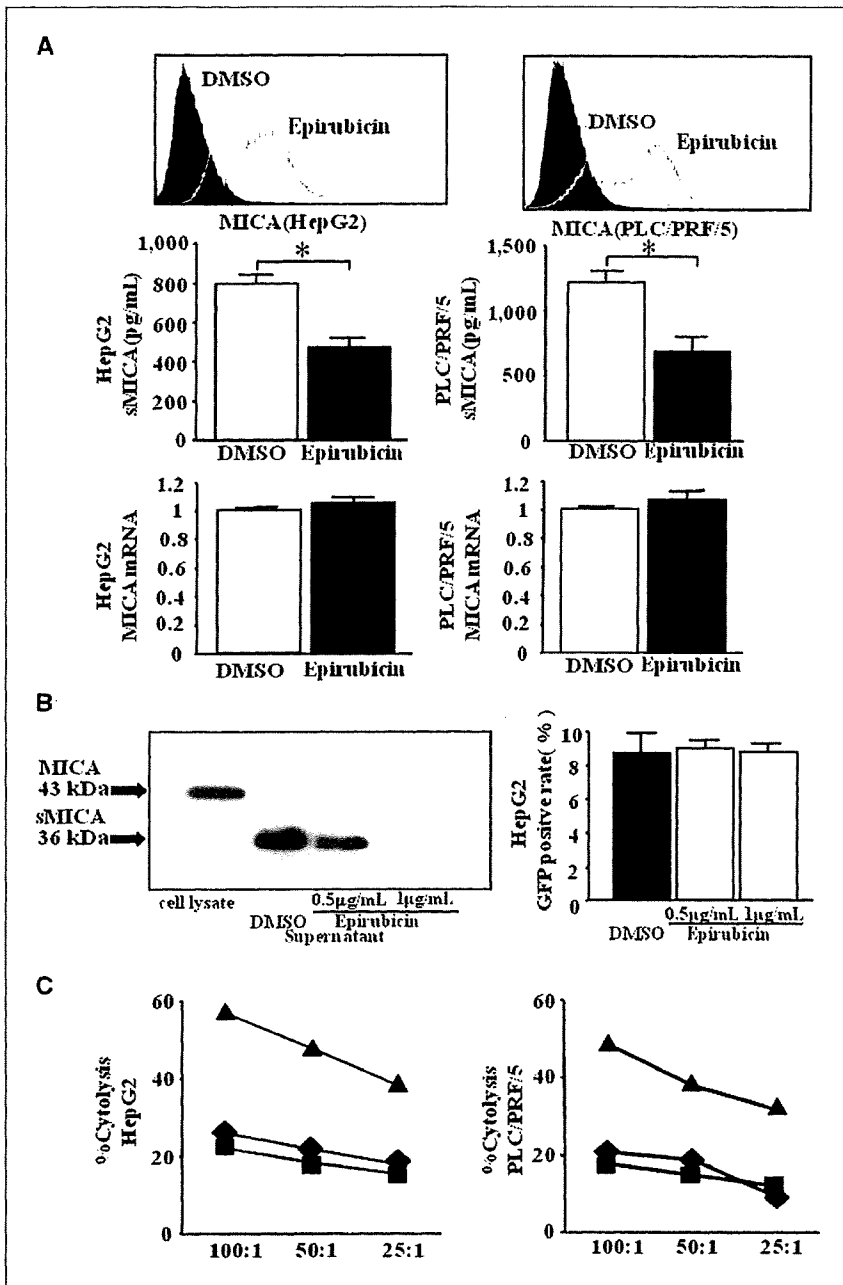


**Figure 4.** Expression and shedding of MICA in epirubicin-treated HCC cells. **A**, HCC cells were treated with a nontoxic dose of 1 µg/mL epirubicin (black lines) or vehicle (DMSO, gray lines) for 24 h and their expression of membrane-bound MICA and MICA mRNA was evaluated by flow cytometry (top panels) and real-time RT-PCR (bottom panels), respectively. Closed histograms, control IgG staining in flow cytometry. At the same time, 24-h culture supernatants were subjected to the analysis of soluble MICA (sMICA) levels by ELISA (middle panels). \*,  $P < 0.05$ . **B**, HepG2 cells were transfected with pMyc-MICA and pEGFP-C1, cultured with 0.5 to 1 µg/mL epirubicin or vehicle (DMSO) for 24 h. Cell lysates from HepG2 cells and 24-h culture supernatants of epirubicin- or vehicle-treated HepG2 cells were immunoprecipitated with anti-Myc. The resulting immunoprecipitates were eluted, treated with N-glycanase, and subjected to Western blot analysis for MICA (left). Transfection efficacies were equal in all treatment groups as evidenced by similar GFP-positive cell rates (right). **C**, the cytolytic activity of NK cells against HCC cells. Vehicle-treated cells (■) or epirubicin-treated cells without (▲) or with blocking antibody of MICA/B (6D4; ◆) were subjected to  $^{51}\text{Cr}$ -release assay. Representative results are shown. Similar results were obtained from three independent experiments.

had been tested with equal variance and Fisher's exact probability test. We defined statistical significance as  $P < 0.05$ .

**Results**

**ADAM10 and CD44 are overexpressed in human HCC.** ADAM10 was detected in all human HCC tissues tested by immunohistochemistry but not in normal liver tissues (Fig. 1A). Flow cytometric analysis revealed that ADAM10 was strongly expressed in a variety of HCC cell lines, including HepG2, PLC/PRF/5 (depicted in Fig. 1B), and Hep3B (data not shown), but faintly in primary hepatocytes. CD44, a typical substrate of the ADAM10 protease, was also expressed in all human HCC tissues

but not in normal liver tissues (Fig. 1A). The data suggest that overexpression of ADAM10 and CD44 is a characteristic of human HCC like other malignancies (22).

**ADAM10 is involved in MICA shedding of HCC cells but ADAM17 is not.** To examine the involvement of ADAM family proteins in MICA ectodomain shedding, ADAM10 or ADAM17 were knocked down in HCC cells using a siRNA-mediated procedure. ADAM10 expression was clearly suppressed in HepG2 cells and PLC/PRF/5 cells at both mRNA and protein levels (Fig. 1B and C). Both cell lines expressed CD44 on the cellular surface and produced significant levels of soluble CD44 (Fig. 1D), indicating that CD44 is expressed and shed from those cell lines. ADAM10 knockdown (KD)

led to an increase in CD44 expression on HCC cells and a decrease in soluble CD44 levels in culture supernatants (Fig. 1D). Because ADAM10 has been established as being a sheddase for CD44, siRNA-mediated knockdown of ADAM10 suppressed not only the expression but also the activity of ADAM10 in HCC cells. HepG2 and PLC/PRF/5 cells also expressed ADAM17, which was clearly knocked down by a siRNA-mediated procedure (Fig. 1B).

HepG2 cells and PLC/PRF/5 cells expressed membrane-bound MICA and also produced soluble MICA (Fig. 2A). Knockdown of ADAM10 for both cell lines clearly upregulated MICA expression on their cellular surface and downregulated soluble MICA levels in their culture supernatant (Fig. 2A). In contrast, knockdown of ADAM17 did not affect the expression of membrane-bound MICA or the production of soluble MICA (Fig. 2B). We also examined the involvement of ADAM17 in MICA shedding of phorbol 12-myristate 13-acetate (PMA)-stimulated HCC cells because ADAM17 is considered to primarily affect stimulated shedding. The expression of membrane-bound MICA and the soluble MICA production were equal between PMA-stimulated ADAM17KD-HCC cells and control HCC cells (Supplementary Fig. S2). Thus, ADAM10, but not ADAM17, is critically involved in the shedding of MICA in HCC cells.

We next evaluated the cytolytic activity of NK cells against HCC cells. The cytolytic activity of NK cells against ADAM10KD-HepG2 cells was higher than that against control HepG2 cells. This activity was inhibited by blocking of anti-MICA/B antibody, suggesting that the increase of NK sensitivity depended on the increased expression of membrane-bound MICA on ADAM10KD-HepG2 cells, although we could not exclude the possibility of the involvement of MICB in this cytotoxicity (Fig. 2C). Similar results were also obtained with ADAM10KD-PLC/PRF/5 cells.

**Epirubicin suppresses ADAM10 expression in HCC cells.** We examined the biological modification of human HCC cells by adding epirubicin, which is commonly used in anti-HCC chemotherapy. We first examined the cytotoxicity of epirubicin to human HCC cells by WST-8 assay. Adding >5  $\mu\text{g}/\text{mL}$  of epirubicin resulted in a significant

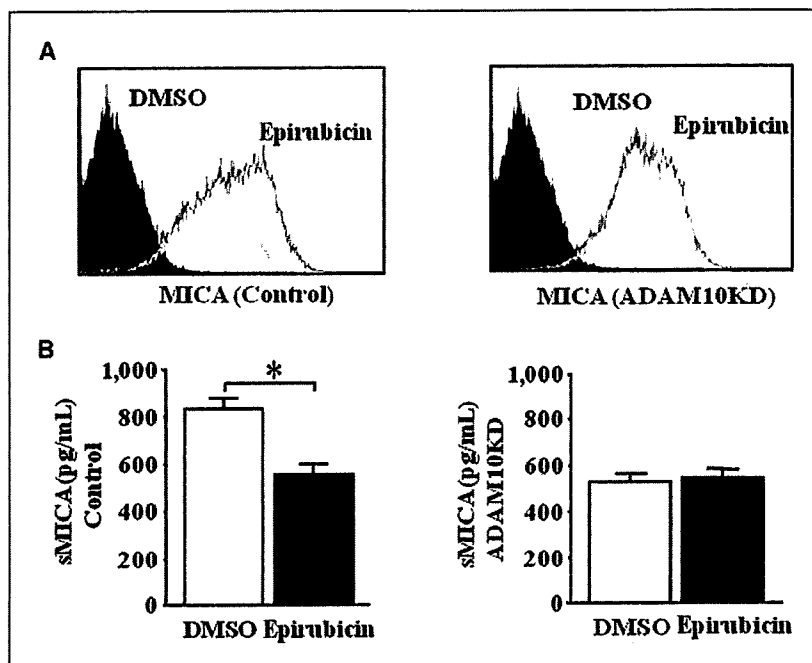
decrease in cell growth of both HepG2 and PLC/PRF/5 cells (Fig. 3B). Based on these findings, we used 1  $\mu\text{g}/\text{mL}$  of epirubicin to evaluate the biological effect on human HCC cells without toxicity. Both HepG2 cells and PLC/PRF/5 cells were cultured for 24 h with epirubicin and then subjected to analysis of ADAM10 expression. Epirubicin suppressed ADAM10 expression at the mRNA and protein levels in both cell lines (Fig. 3C). Although the data are not shown, doxorubicin also suppressed ADAM10 expression in HCC cells.

**Epirubicin inhibits MICA ectodomain shedding and enhances susceptibility to NK cells of HCC cells.** The above observations led us to investigate whether epirubicin or doxorubicin treatment would affect MICA ectodomain shedding in HCC cells. Epirubicin treatment led to an increase in membrane-bound MICA expression and a decrease in soluble MICA production in both HepG2 and PLC/PRF/5 cells (Fig. 4A). The mRNA levels of MICA did not change after exposure to epirubicin in both HCC cells (Fig. 4A). Similar data were obtained with doxorubicin-treated cells (data not shown).

To confirm whether the soluble MICA detected by ELISA was actually reflected in the cleaved form, we transfected Myc-tagged MICA into HepG2 cells and collected culture supernatants as well as cellular lysates. Immunoprecipitates from these samples with anti-Myc were subjected to Western blot analysis after treatment with N-glycosidase. MICA in the culture supernatants migrated faster than cellular MICA (Fig. 4B), indicating that the MICA detected by ELISA is actually processed and released from full-length MICA. Epirubicin treatment led to a decrease in soluble MICA protein in HepG2 cells (Fig. 4B).

We next evaluated whether the epirubicin treatment could also modify the NK sensitivity of human HCC cells. Epirubicin-treated HepG2 cells or PLC/PRF/5 cells were more susceptible to NK cells than nontreated HepG2 or PLC/PRF/5 cells (Fig. 4C). The cytolytic activity against epirubicin-treated HCC cells was significantly decreased to the control levels by adding the anti-MICA/B blocking antibody. These results showed that the addition of epirubicin enhanced the NK sensitivity of HCC cell through increased

**Figure 5.** The epirubicin-mediated modification of MICA is ADAM10 dependent. HepG2 cells were transfected with ADAM10 siRNA (*ADAM10KD*) or control siRNA (*Control*) and further cultured with 1  $\mu\text{g}/\text{mL}$  of epirubicin (*black lines*) or vehicle (DMSO, *gray line*) for 24 h. The expression of membrane-bound MICA (*MICA*) was evaluated by flow cytometry (A), and the soluble MICA (*sMICA*) production in the culture supernatant was evaluated by specific ELISA (B). Similar results were obtained from two independent experiments. \*,  $P < 0.05$ .



expression of membrane-bound MICA, although the possibility of MICB involvement could not be excluded. The doxorubicin-treated human HCC cells showed similar results to those obtained from epirubicin-treated HCC cells (data not shown).

**Epirubicin inhibits MICA ectodomain shedding through suppression of ADAM10.** To examine whether the suppressive effect of epirubicin on MICA shedding occurred through downregulation of ADAM10, HepG2 cells were transfected with ADAM10 siRNA or scramble siRNA as a control and then treated with epirubicin. Consistent with earlier observations, epirubicin upregulated MICA surface expression and downregulated the levels of soluble MICA in control cells (Fig. 5). In contrast, neither upregulation of surface MICA nor downregulation of soluble MICA levels was observed in ADAM10KD-HepG2 cells. These results suggest that the suppressive effect of epirubicin on MICA shedding is mediated by ADAM10 downregulation. We also found similar results with ADAM10KD-PLC/PRF/5 cells (data not shown).

**Soluble CD44 and soluble MICA levels in patients with HCC.** We have shown that ADAM10 is expressed in human HCC tissues. However, it is not clear whether ADAM10 activity in HCC tissues is actually involved in MICA shedding in patients. Because ADAM10 was reported to be the constitutive functional sheddase of CD44 (23), we examined the soluble CD44 levels in HCC patients, which might be produced from tumor cells through ADAM10 activity. As shown in Fig. 6A, the soluble CD44 levels in HCC patients ( $n = 97$ ) were significantly higher than those in age-matched healthy volunteers ( $n = 32$ ). More importantly, soluble MICA levels in HCC patients significantly correlated with soluble CD44 levels (Fig. 6B), suggesting a close link between MICA shedding and ADAM10 activity.

We further examined soluble CD44 levels before and 2 weeks after TACE in HCC patients. Whereas the levels did not change in nontreated HCC patients during the 2-week interval ( $n = 9$ ;  $306.7 \pm 82.5$  ng/mL and  $309.9 \pm 79.9$  ng/mL after 2 weeks), they were significantly decreased in epirubicin-based TACE-treated HCC patients ( $n = 21$ ;  $339.7 \pm 78.1$  ng/mL before TACE and  $308.9 \pm 81.4$  ng/mL after TACE,  $P < 0.003$ ). The changes of soluble CD44 in TACE treatment correlated significantly with those of soluble MICA ( $P = 0.0002$ ; Fig. 6C). These results indicated that ADAM10-mediated CD44 shedding was decreased after TACE in HCC patients, implying that this reduction of ADAM10 activity might be related to the decline in MICA shedding.

## Discussion

MICA shedding is thought to be a principal mechanism by which tumor cells escape from NKG2D-mediated immunosurveillance (13). Thus, inhibition of MICA shedding should be a reasonable strategy for enhancing antitumor immunity. In the present study, we showed that ADAM10 was overexpressed in human HCC tissues and that ADAM10 knockdown resulted in increased expression of membrane-bound MICA, decreased production of soluble MICA, and upregulation of NK sensitivity of human HCC cells. These results point to ADAM10 as a therapeutic target for inhibiting MICA shedding, thereby ameliorating immunity against HCC. Waldhauer and colleagues recently showed that both ADAM10 and ADAM17 proteases are critically involved in the proteolytic release of soluble MICA of human 293T fibroblast cells and HeLa cervix carcinoma cells (20). Interestingly, in the present study, ADAM17 knockdown failed to affect MICA expression in human HepG2 cells or PLC/PRF/5 cells. Thus, ADAM10, not ADAM17, plays an essential role in the shedding of MICA in human HCC cells. Andereg and colleagues

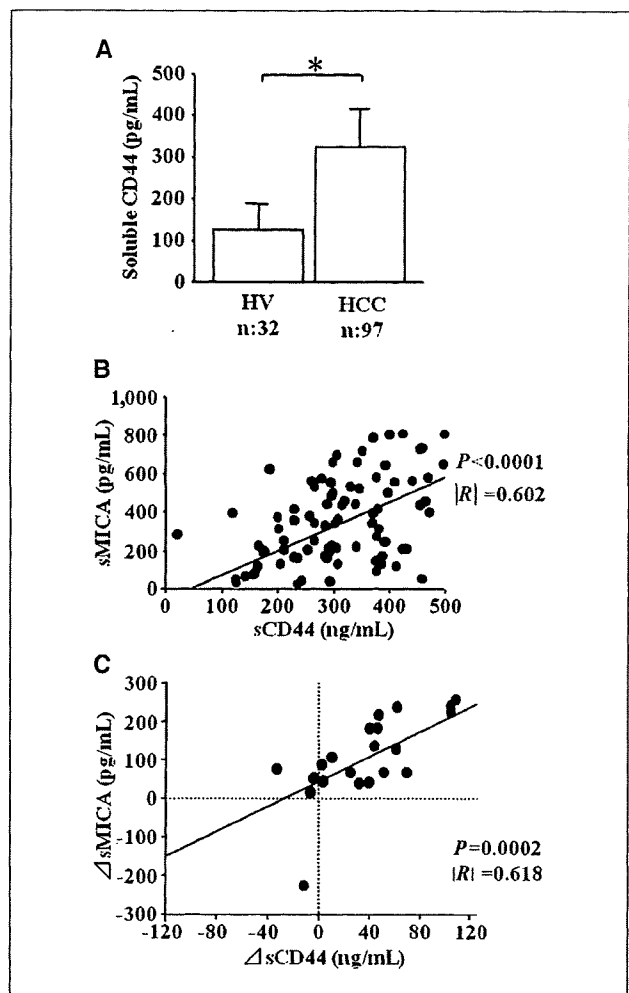


**Figure 6.** Correlation between soluble CD44 and soluble MICA in human HCC patients. **A** and **B**, soluble CD44 levels and MICA levels in healthy volunteers and HCC patients. Soluble CD44 levels ( $sCD44$ ) and soluble MICA levels ( $sMICA$ ) were determined for sera of HCC patients ( $n = 97$ ) and age-matched healthy volunteers ( $HV$ ;  $n = 32$ ). **A**, comparison of  $sCD44$  levels in healthy volunteers and HCC patients. **B**, correlation between  $sCD44$  levels and  $sMICA$  levels in 97 HCC patients. \*,  $P < 0.05$ . **C**, correlation of  $sCD44$  levels and  $sMICA$  levels during TACE therapy. HCC patients ( $n = 21$ ) treated with epirubicin-based TACE therapy were enrolled and examined for  $sMICA$  and  $sCD44$  levels before and 2 wk after therapy. Changes in  $sMICA$  ( $\Delta sMICA =$  serum level of  $sMICA$  before TACE treatment – serum level of  $sMICA$  after TACE treatment) and those in  $sCD44$  levels ( $\Delta sCD44 =$  serum level of  $sCD44$  before TACE treatment – serum level of  $sCD44$  after TACE treatment) are plotted.

(23) reported that only ADAM10, not ADAM17, contributed to shedding of CD44 molecules in human melanoma cells although both ADAM10 and ADAM17 proteases were significantly expressed in human melanoma tissues, suggesting that ADAM10 and ADAM17 do not always work in a similar manner. A recent report showed that ADAM10, but not ADAM17, could directly bind to calmodulin (24), which may involve the difference of MICA cleavage between ADAM10 and ADAM17 proteases. Recently, Boutet and colleagues reported that ADAM17 regulates proteolytic shedding of the MICB protein, which is another ligand for the NKG2D receptor on immune cells (25). We previously showed that both soluble MICA and MICB significantly increased in the sera of HCC patients and that therapeutic intervention for HCC leads to reduction of soluble

MICA levels, but not of soluble MICB levels (17), suggesting a more important role of soluble MICA in regulating NKG2D expression after HCC therapy. This led us to focus on the mechanism of MICA shedding in the present study.

Our results revealed that anticancer drugs such as epirubicin and doxorubicin downregulated ADAM10 expression and activity, thereby inhibiting MICA ectodomain shedding. The ADAM family proteins, which are highly expressed in some tumors, play a role in secreting growth factors, such as HB-EGF, and migration of cells. Thus, it is speculated that these proteins could be potential targets for tumor treatment (22). The present study is the first to show that clinically available anticancer drugs have an ability to modulate the expression of ADAM family proteins. They seem to suppress ADAM10 expression at a transcriptional level, but the precise mechanism of this suppression is not yet known.

The MICA ELISA system may not equally detect all soluble MICA (MICA molecules have >60 allelic variants). Our finding that soluble MICA could be detected in all HCC patients suggests that this system was applicable for our cohort of HCC patients. However, special caution should be paid for the use of this ELISA system for widely polymorphic MICA. Because CD44 is well known to be released into circulation from tumors by proteolytic cleavage of ADAM10 (23), the activity of ADAM10 in HCC tissues may be correlated with soluble CD44 levels. If so, our data suggest a close link between ADAM10 activity and the shedding of MICA in HCC. Furthermore, the decline in soluble MICA levels correlated well with the decline in soluble CD44 levels as early as 2 weeks after epirubicin-based TACE therapy. Reducing the tumor volume by such therapy may have led to both decreases but it is also possible that epirubicin suppresses ADAM10 activity, thereby inhibiting the shedding of MICA and CD44. Epirubicin may have a previously unrecognized role in cancer therapy; that is, affecting ADAM10 activity and MICA shedding rather than simply serving as a direct toxic agent for tumor cells.

Our data suggest that anti-HCC chemotherapy could remodel HCC cells, enhancing sensitivity to NK cells by upregulating MICA

expression on the cellular surface. A concomitant decline in soluble MICA levels ameliorates NK cell ability by upregulating its NKG2D expression. We previously showed that activation of local innate antitumor immunity in liver tissues resulted in eliciting tumor-specific acquired immunity (21). If liver innate immunity is efficiently activated after anti-HCC chemotherapy, an additional antitumor effect against HCC cells could be expected. Immune modulators such as  $\alpha$ -galactosylceramide have been shown to efficiently activate liver innate immune cells, including NK cells (21, 26). The combination therapy of anti-HCC chemotherapy and immunotherapy targeting NK cells might improve the antitumor effect of unresectable HCC and the prognosis of HCC patients.

In spite of recent progress in HCC therapies, there remains significant room for improvement, especially with respect to advanced liver cancer. We have shown here that anti-HCC chemotherapy resulted in enhanced NK sensitivity of HCC cells through inhibition of the activity of ADAM10 protease followed by modification of MICA expression. These findings indicate that efficient activation of liver innate immunity after anti-HCC chemotherapy might represent a particularly promising approach to suppress tumor growth and promote regression in liver cancer patients.

## Disclosure of Potential Conflicts of Interest

No potential conflicts of interest were disclosed.

## Acknowledgments

Received 3/4/09; revised 7/15/09; accepted 7/24/09; published OnlineFirst 10/13/09.  
**Grant support:** Grant-in-Aid from the Ministry of Education, Culture, Sports, Science and Technology of Japan (T. Takehara) and Grant-in-Aid for Research on Hepatitis and BSE from the Ministry of Health, Labour and Welfare of Japan (N. Hayashi).  
 The costs of publication of this article were defrayed in part by the payment of page charges. This article must therefore be hereby marked *advertisement* in accordance with 18 U.S.C. Section 1734 solely to indicate this fact.

## References

- Fattovich G, Stroffolini T, Zagni I, Donato F. Hepatocellular carcinoma in cirrhosis: incidence and trends. *Gastroenterology* 2004;127:S35-50.
- Bosch FX, Ribes J, Diaz M, Cleries R. Primary liver cancer: worldwide incidence and trends. *Gastroenterology* 2004;127:S5-16.
- Takayasu K, Arai S, Ikai I, et al. Prospective cohort study of transarterial chemoembolization for unresectable hepatocellular carcinoma in 8510 patients. *Gastroenterology* 2006;131:461-9.
- Doherty DG, O'Farrelly C. Innate and adaptive lymphoid cells in human liver. *Immunol Rev* 2006;174:5-20.
- Mehal WZ, Azzaroli F, Crispe IN. Immunology of the healthy liver: old questions and new insights. *Gastroenterology* 2001;120:250-60.
- Bauer S, Groh V, Wu J, et al. Activation of NK cells and T cells by NKG2D, a receptor for stress-inducible MICA. *Science* 1999;285:727-9.
- Groh V, Rhinehart R, Seceist H, Bauer S, Grabstein KH, Spies T. Broad tumor-associated expression and recognition by tumor-derived  $\gamma$ T cells of MICA and MICB. *Proc Natl Acad Sci U S A* 1999;96:6879-84.
- Jinushi M, Takehara T, Tatsumi T, et al. Expression of MICA and MICB in human hepatocellular carcinomas and their regulation by retinoic acids. *Int J Cancer* 2003;104:354-61.
- Wu JD, Higgins LM, Steinle A, Cosman D, Haugk K, Plymate SR. Prevalent expression of the immunostimulatory MHC class I chain-related molecule is counteracted by shedding in prostate cancer. *J Clin Invest* 2004;114:560-8.
- Raffaghello L, Prigione I, Airoldi I, et al. Downregulation and/or release of NKG2D ligands as an immune evasion strategy of human neuroblastoma. *Neoplasia* 2004;6:558-68.
- Ogasawara K, Lanier LL. NKG2D in NK and T cell-mediated immunity. *J Clin Immunol* 2005;25:534-40.
- Coudert JD, Held W. The role of the NKG2D receptor for tumor immunity. *Semin Cancer Biol* 2006;16:333-43.
- Groh V, Wu J, Yee C, Spies T. Tumor-derived soluble MIC ligands impair expression of NKG2D and T cell activation. *Nature* 2002;419:734-8.
- Salih HR, Rammensee HG, Steinle A. Downregulation of MICA on human tumors by proteolytic shedding. *J Immunol* 2002;169:4098-102.
- Salih HR, Antropius H, Gieseke F, et al. Functional expression and release of ligands for activating immunoreceptor NKG2D in leukemia. *Blood* 2003;102:1389-96.
- Jinushi M, Takehara T, Tatsumi T, et al. Impairment of natural killer cell and dendritic cell functions by soluble form of MHC class I-related chain A in advanced human hepatocellular carcinoma. *J Hepatol* 2005;43:1013-20.
- Kohga K, Takehara T, Tatsumi T, et al. Serum levels of soluble major histocompatibility complex (MHC) class I-related chain A in patients with chronic liver disease and changes during transcatheter arterial embolization for hepatocellular carcinoma. *Cancer Sci* 2008;99:1643-9.
- Holdenrieder S, Stieber P, Peterfi A, Nagel D, Steinle A, Salih HR. Soluble MICA in malignant disease. *Int J Cancer* 2006;118:684-7.
- Kaiser BK, Yim D, Chow IT, et al. Disulphide-isomerase-enabled shedding of tumor-associated NKG2D ligands. *Nature* 2007;447:482-6.
- Waldhauer I, Goehlsdorf D, Gieseke F, et al. Tumor-associated MICA is shed by ADAM proteases. *Cancer Res* 2008;68:6368-76.
- Tatsumi T, Takehara T, Yamaguchi S, et al. Intrahepatic delivery of  $\alpha$ -galactosylceramide-pulsed dendritic cells suppresses liver tumor. *Hepatology* 2007;45:22-30.
- Mochizuki S, Okada Y. ADAMs in cancer cell proliferation and progression. *Cancer Sci* 2007;98:161-7.
- Andereg U, Eichenberg T, Parthaune T, et al. Simon JC. ADAM10 is the constitutive functional sheddase of CD44 in human melanoma cells. *J Invest Dermatol* 2009;129:1471-82.
- Nagano O, Murakami D, Hartmann D, et al. Cell-matrix interaction via CD44 is independently regulated by different metalloproteinases activated in response to extracellular domain  $Ca^{2+}$  influx and PKC activation. *J Cell Biol* 2004;165:893-902.
- Boutef P, Aguera-Gonzalez S, Atkinson S, et al. The metalloproteinase ADAM17/TNF- $\alpha$  enzyme regulates proteolytic shedding of the MHC class I-related chain B protein. *J Immunol* 2009;182:49-53.
- Miyagi T, Takehara T, Tatsumi T, et al. CD1d-mediated stimulation of natural killer T cells selectively activates hepatic natural killer cells to eliminate experimentally disseminated hepatoma cells in murine liver. *Int J Cancer* 2003;106:81-9.



## BH3-Only Protein Bid Participates in the Bcl-2 Network in Healthy Liver Cells

Hayato Hikita,<sup>1\*</sup> Tetsuo Takehara,<sup>1\*</sup> Takahiro Kodama,<sup>1</sup> Satoshi Shimizu,<sup>1</sup> Atsushi Hosui,<sup>1</sup> Takuya Miyagi,<sup>1</sup> Tomohide Tatsumi,<sup>1</sup> Hisashi Ishida,<sup>1</sup> Kazuyoshi Ohkawa,<sup>1</sup> Wei Li,<sup>1</sup> Tatsuya Kanto,<sup>1</sup> Naoki Hiramatsu,<sup>1</sup> Lothar Hennighausen,<sup>2</sup> Xiao-Ming Yin,<sup>3</sup> and Norio Hayashi<sup>1</sup>

Bcl-2 homology domain 3 (BH3)-only protein Bid is posttranslationally cleaved by caspase-8 into its truncated form (tBid) and couples with stress signals to the mitochondrial cell death pathway. However, the physiological relevance of Bid is not clearly understood. Hepatocyte-specific knockout (KO) of Bcl-xL leads to naturally-occurring apoptosis despite co-expression of Mcl-1, which shares a similar anti-apoptotic function. We generated Bcl-xL KO, Bcl-xL/Bid double KO, Bcl-xL/Bak double KO, Bcl-xL/Bax double KO, and Bcl-xL/Bak/Bax triple KO mice and found that hepatocyte apoptosis caused by Bcl-xL deficiency was completely dependent on Bak and Bax, and surprisingly on Bid. This indicated that, in the absence of Bid, Bcl-xL is not required for the integrity of differentiated hepatocytes, suggesting a complicated interaction between core Bcl-2 family proteins and BH3-only proteins even in a physiological setting. Indeed, a small but significant level of tBid was present in wild-type liver under physiological conditions. tBid was capable of binding to Bcl-xL and displacing Bak and Bax from Bcl-xL, leading to release of cytochrome c from wild-type mitochondria. Bcl-xL-deficient mitochondria were more susceptible to tBid-induced cytochrome c release. Finally, administration of ABT-737, a pharmacological inhibitor of Bcl-2/Bcl-xL, caused Bak/Bax-dependent liver injury, but this was clearly ameliorated with a Bid KO background. **Conclusion:** Bid, originally considered to be a sensor for apoptotic stimuli, is constitutively active in healthy liver cells and is involved in the Bak/Bax-dependent mitochondrial cell death pathway. Healthy liver cells are addicted to a single Bcl-2-like molecule because of BH3 stresses, and therefore special caution may be required for the use of the Bcl-2 inhibitor for cancer therapy. (HEPATOLOGY 2009;50:1972-1980.)

Abbreviations: ALT, alanine aminotransferase; BH3, Bcl-2 homology domain 3; KO, knockout; tBid, truncated form of Bid; TNE, tumor necrosis factor; TUNEL, terminal deoxynucleotidyl transferase-mediated 2'-deoxyuridine 5'-triphosphate nick-end labeling.

From the <sup>1</sup>Department of Gastroenterology and Hepatology, Osaka University Graduate School of Medicine, Osaka, Japan; <sup>2</sup>Laboratory of Genetics and Physiology, National Institute of Diabetes and Digestive and Kidney Diseases, National Institute of Health, Bethesda, MD; and the <sup>3</sup>Department of Pathology, University of Pittsburgh School of Medicine, Pittsburgh, PA.

\*These authors contributed equally to this work and share first authorship.

Received May 20, 2009; accepted July 21, 2009.

Supported in part by a Grant-in-Aid for Scientific Research from the Ministry of Education, Culture, Sports, Science, and Technology, Japan (to T. Takehara).

Address reprint requests to: Norio Hayashi, M.D., Ph.D., Department of Gastroenterology and Hepatology, Osaka University Graduate School of Medicine, 2-2 Yamada-oka, Suita, Osaka 565-0871, Japan. E-mail: hayashin@gh.med.osaka-u.ac.jp; fax: (81)-6-6879-3629.

Copyright © 2009 by the American Association for the Study of Liver Diseases.

Published online in Wiley InterScience (www.interscience.wiley.com).

DOI 10.1002/hep.23207

Potential conflict of interest: Nothing to report.

Additional Supporting Information may be found in the online version of this article.

Bcl-2 family proteins regulate the mitochondrial pathway of apoptosis in mammalian cells.<sup>1</sup> They are divided into two basic groups: core Bcl-2 family proteins and Bcl-2 homology domain 3 (BH3)-only proteins. Core Bcl-2 family proteins have three or four Bcl-2 homology domains (BH1-BH4 domains), referred to as multidomain members, and structural similarity. These proteins display opposing bioactivities from inhibition to promotion of apoptosis and can be further divided into two groups: anti-apoptotic members, including Bcl-2, Bcl-xL, Bcl-w, Mcl-1, and Bfl-1, and pro-apoptotic members, including Bax and Bak. Pro-apoptotic Bak and Bax are effector molecules of the Bcl-2 family and induce release of cytochrome c from mitochondria, presumably through their ability to form pores at the mitochondrial outer membrane. Anti-apoptotic members, which serve as regulators, inhibit Bak and Bax. The original rheostat model argues for a fine balance between Bax-like pro-apoptotic proteins and Bcl-2-like an-

ti-apoptotic proteins in defining life and death, and this balance would be equal or favor survival in a healthy cell.<sup>2</sup>

BH3-only proteins consist of at least eight members and only share homology with each other and the core Bcl-2 family proteins through the short BH3 motif. They are transcriptionally induced or posttranslationally activated in response to a variety of apoptotic stimuli.<sup>3</sup> When they are induced or activated, they interact with core Bcl-2 family proteins and set the rheostat balance toward apoptosis by directly activating Bax-like molecules or neutralizing Bcl-2-like molecules.<sup>4</sup> Therefore, they serve as initial sensors of apoptotic signals that emanate from various cellular processes. Bid, a member of the BH3-only proteins, is activated via caspase-8-mediated cleavage in response to ligation of the death receptor, and its N-terminal truncated form (tBid) translocates to mitochondria and activates the mitochondrial death pathway.<sup>5</sup> In so-called type 1 cells, such as lymphoid cells, Fas activation leads to caspase-8 activation followed by direct activation of downstream caspases such as caspase-3 and caspase-7, where Bid does not have significant roles.<sup>6</sup> In contrast, in type 2 cells, Fas-mediated activation of caspase-8 is not enough to activate downstream caspases. In those cells, tBid links the extrinsic or death-receptor pathway to the intrinsic or mitochondrial pathway to execute apoptosis. Hepatocytes are identified as a typical type 2 cell in which Bid plays a critical role in receptor-mediated cell death pathways.<sup>7</sup>

In our previous research, we found that genetic ablation of Bcl-xL in hepatocytes causes spontaneous apoptosis in mice.<sup>8</sup> This indicates that Bcl-xL is a critical apoptosis antagonist in adult healthy hepatocytes, although they possess other anti-apoptotic members of the Bcl-2 family such as Mcl-1. This might be simply explained by the fact that the absence of Bcl-xL affects the rheostat balance of core Bcl-2 family proteins by increasing the ratio of Bax and Bak to anti-apoptotic Bcl-2 proteins. Indeed, neuronal cell death during development caused by Bcl-xL deficiency is ameliorated by loss of Bax.<sup>9</sup> Platelet cell death caused by Bcl-xL deficiency is also ameliorated by loss of Bak.<sup>10</sup> These studies indicate that the stoichiometry between Bcl-xL and Bax or Bak dictates cellular fate. However, the possibility of BH3-only proteins being involved in the apoptosis rheostat in healthy cells has not been addressed. We generated Bcl-xL/Bid double-knockout (KO) mice and demonstrated that apoptosis caused by Bcl-xL deficiency is critically dependent on Bid. A small amount of Bid appears to be activated in the liver under physiological conditions and to be significant for inducing cytochrome c release from Bcl-xL-deficient mitochondria. This study shed light on the active participation of BH3-only proteins, which are generally

considered to be sensors of apoptotic stimuli, in the Bcl-2 network regulating life and death of healthy differentiated hepatocytes.

## Materials and Methods

**Mice.** Mice carrying a *bcl-x* gene with 2 loxP sequencers at the promoter region and a second intron (*bcl-x<sup>lox/lox</sup>*) were described previously.<sup>11</sup> Heterozygous AlbCre transgenic mice expressing Cre recombinase gene under the promoter of the albumin gene<sup>8</sup> and traditional Bid KO mice<sup>7</sup> also have been described previously. We purchased from the Jackson Laboratory (Bar Harbor, ME) traditional Bak KO mice, traditional Bax KO mice, and conditional Bak/Bax KO mice (*bak<sup>-/-</sup> bax<sup>lox/lox</sup>*).<sup>12</sup> We generated hepatocyte-specific Bcl-xL KO mice (*bcl-x<sup>lox/lox</sup> AlbCre*), Bcl-xL/Bid double-KO mice (*bid<sup>-/-</sup> bcl-x<sup>lox/lox</sup> AlbCre*), Bcl-xL/Bak double-KO mice (*bak<sup>-/-</sup> bcl-x<sup>lox/lox</sup> AlbCre*), Bcl-xL/Bax double-KO mice (*bax<sup>-/-</sup> bcl-x<sup>lox/lox</sup> AlbCre*), and Bcl-xL/Bak/Bax triple-KO mice (*bak<sup>-/-</sup> bax<sup>lox/lox</sup> bcl-x<sup>lox/lox</sup> AlbCre*) by mating the strains. They were maintained in a specific pathogen-free facility and treated with humane care under approval from the Animal Care and Use Committee of Osaka University Medical School.

**Apoptosis Assay.** The levels of serum alanine aminotransferase (ALT) were measured by a standard method, and serum caspase-3/7 activity was measured by a luminescent substrate assay for caspase-3 and caspase-7 (Caspase-Glo assay, Promega, Tokyo, Japan). The caspase-3/7 activity was normalized by each control group. For histological analysis, the liver sections were stained with hematoxylin-eosin. To detect cells with oligonucleosomal DNA breaks, the sections were also subjected to terminal deoxynucleotidyl transferase-mediated deoxyuridine triphosphate nick-end labeling (TUNEL) staining, according to a previously reported procedure.<sup>13</sup>

**Western Blot Analysis.** Liver tissue was lysed with a lysis buffer (1% Nonidet P-40, 0.5% sodium deoxycholate, 0.1% sodium dodecyl sulfate, 1 × protein inhibitor cocktail (Nacalai tesque, Kyoto, Japan), phosphate-buffered saline, pH 7.4). Equal amounts of protein were electrophoretically separated by sodium dodecyl sulfate polyacrylamide gels and transferred onto polyvinylidene fluoride membrane. For immunodetection, the following antibodies were used: anti-Bcl-xL antibody (Santa Cruz Biotechnology, Santa Cruz, CA), anti-Mcl-1 antibody (Rockland, Gilbertsville, PA), previously described anti-Bid antibody generated from glutathion-S-transferase-Bid fusion protein,<sup>14</sup> anti-full-length Bid antibody, anti-cleaved caspase-7 antibody, anti-Bax antibody, anti-Cox IV antibody (Cell Signaling Technology, Beverly, MA),

anti-Bak antibody (Millipore, Billerica, MA), and anti- $\beta$ -actin antibody (Sigma-Aldrich, St. Louis, MO).

**Isolation of Mitochondria-Rich and Cytosolic Fraction.** After liver tissue was homogenized using isolation buffer (225 mM mannitol, 75 mM sucrose, 0.1 mM ethylene glycol tetraacetic acid, 1 mg/mL fatty acid-free bovine serum albumin,  $1 \times$  protein inhibitor cocktail, 10 mM 4-(2-hydroxyethyl)-1-piperazine ethanesulfonic acid-potassium hydroxide, pH 7.4), the lysate was centrifuged at 600g for 10 minutes, and the supernatant was centrifuged at 15,000g for 10 minutes. The pellet was regarded as a mitochondria-rich fraction and the supernatant as a cytosolic fraction.

**Immunoprecipitation of Bcl-xL.** Approximately 30 mg liver tissue was lysed with a TNE buffer (1% Nonidet P-40, 1 mM ethylenediaminetetra-acetic acid,  $1 \times$  protein inhibitor cocktail, 0.15 M NaCl, 10 mM Tris-HCl, pH 7.8). Equal amounts of protein samples were rotated with protein G sepharose (GE Healthcare, Tokyo, Japan) and anti-Bcl-xL antibody (Abcam, Cambridge, MA) overnight at 4°C. After centrifugation, the pellet was collected as the immunoprecipitate protein.

**Incubation of tBid or Bid for Immunoprecipitation.** Liver tissue (90 mg) was lysed with 800  $\mu$ L lysis buffer (2 mM ethylenediaminetetra-acetic acid, 10 mM ethylene glycol tetra-acetic acid, 50 mM NaF, 5 mM Na<sub>2</sub>P<sub>4</sub>O<sub>7</sub>, 10 mM  $\beta$ -glycerophosphate, 0.1% 2-mercaptoethanol, 1% Triton X,  $1 \times$  protein inhibitor cocktail, 50 mM Tris-HCl, pH 7.5). Equal volumes of protein samples were incubated with or without recombinant mouse tBid or full-length Bid (R&D Systems, Minneapolis, MN).

**Analysis of Cytochrome C Release.** The mitochondria-rich fraction was diluted in a mitochondria dilution buffer (395 mM sucrose, 0.1 mM ethylene glycol tetraacetic acid, 10 mM 4-(2-hydroxyethyl)-1-piperazine ethanesulfonic acid-potassium hydroxide, pH 7.4). The diluted mitochondria were incubated with recombinant mouse tBid or full-length Bid diluted with a reaction buffer (125 mM KCl, 0.5 mM MgCl<sub>2</sub>, 3.0 mM succinic acid, 3.0 mM glutamic acid, 10 mM 4-(2-hydroxyethyl)-1-piperazine ethanesulfonic acid-potassium hydroxide,  $1 \times$  protein inhibitor cocktail, 2.5 mM ethylenediaminetetra-acetic acid and BOC-Asp (OMe) CH<sub>2</sub>F 20  $\mu$ M, pH 7.4) for 30 minutes at 37°C. The levels of cytochrome c in the buffer were determined using an enzyme-linked immunosorbent assay kit (R&D Systems). The maximum or spontaneous release of cytochrome c was defined as the level of samples incubated with 0.1% Triton X-100 or medium alone, respectively. The percentage release of cytochrome c was calculated using the following formula:

% release = (experimental release - spontaneous release)  $\times$  100/(maximum release - spontaneous release).

**ABT-737 Injection Study.** ABT-737 was provided

by Abbott Laboratories (Abbott, Park, IL). ABT-737 was dissolved with a mixture of 30% propylene glycol, 5% Tween 80, and 65% D5W (5% dextrose in water), final pH 4 to 5. Mice were given a single intraperitoneal injection of ABT-737 at 100 mg/kg and sacrificed 16 hours later. Platelets were counted using an automated cell counter (Sysmex, Kobe, Japan).

**Statistical Analysis.** Data are presented as mean  $\pm$  standard deviation. Multiple comparisons of TUNEL-positive cells were performed by analysis of variance followed by Fisher's *post hoc* correction. The other multiple comparisons were performed by analysis of variance followed by Scheffe *post hoc* correction.  $P < 0.05$  was considered statistically significant.

## Results

### Hepatocyte Apoptosis Caused by Bcl-xL Deficiency Is Completely Lost with Bid-Deficient Background.

To examine the possibility of whether Bid is involved in apoptosis caused by Bcl-xL deficiency, hepatocyte-specific Bcl-xL KO mice were crossed with traditional Bid KO mice. After mating *bid*<sup>+/-</sup> *bcl-x*<sup>flx/flx</sup> *AlbCre* mice with *bid*<sup>+/-</sup> *bcl-x*<sup>flx/flx</sup> mice, western blot analysis confirmed lack of Bcl-xL and Bid in the liver of Bcl-xL KO mice and Bid KO mice, respectively, and intermediate expression of Bid in the Bid +/- liver (Fig. 1A). Consistent with our previous findings,<sup>8</sup> Bcl-xL KO mice (*bid*<sup>+/+</sup> *bcl-x*<sup>flx/flx</sup> *AlbCre*) produced spontaneous hepatocyte apoptosis (Fig. 1B), which was associated with caspase-7 activation in the liver (Fig. 1C). Serum ALT levels (Fig. 1D), caspase-3/7 activity (Fig. 1E), and the frequency of TUNEL-positive hepatocytes (Fig. 1F) were significantly higher in Bcl-xL KO mice than in wild-type mice (*bid*<sup>+/+</sup> *bcl-x*<sup>flx/flx</sup>). Bid KO mice (*bid*<sup>-/-</sup> *bcl-x*<sup>flx/flx</sup>) did not produce any liver phenotypes under physiological conditions, in agreement with a previous report.<sup>7</sup> This was further confirmed by our additional analysis on Bid KO mice and control littermates, which showed no difference in serum ALT levels (Supporting Fig. 1A), caspase-3/7 activity (Supporting Fig. 1B), and the ratios of liver weight to body weight (Supporting Fig. 1C). Of importance is the finding that serum ALT levels were reduced to the normal levels in Bcl-xL/Bid double-KO mice (*bid*<sup>-/-</sup> *bcl-x*<sup>flx/flx</sup> *AlbCre*). Bcl-xL KO with Bid heterozygosity (*bid*<sup>+/-</sup> *bcl-x*<sup>flx/flx</sup> *AlbCre*) displayed intermediate ALT levels between Bcl-xL KO mice and double-KO mice. In agreement with this observation, the number of TUNEL-positive hepatocytes in Bcl-xL/Bid double-KO mice reached background levels. In addition, the levels of caspase-3/7 activity in serum were also normalized in Bcl-xL/Bid double-KO mice. Taken together, these observations indicated that

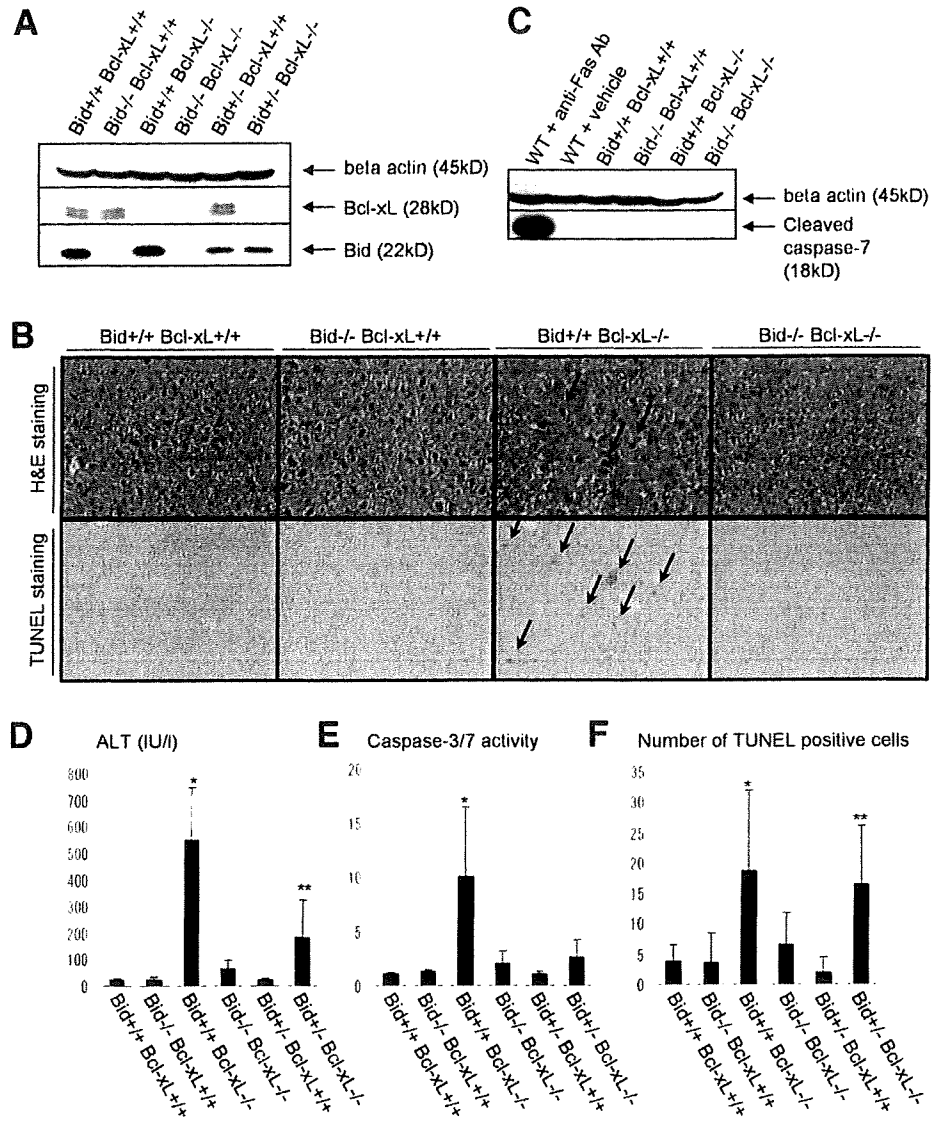


Fig. 1. Bcl-xL/Bid double-KO mice. Offspring from mating *bid*<sup>+/+</sup> *bcl-x*<sup>fllox/fllox</sup> *AlbCre* mice and *bid*<sup>+/+</sup> *bcl-x*<sup>fllox/fllox</sup> mice were sacrificed at 6 weeks after birth. Bcl-xL<sup>+/+</sup> stands for *bcl-x*<sup>fllox/fllox</sup> without *AlbCre*, and Bcl-xL<sup>-/-</sup> stands for *bcl-x*<sup>fllox/fllox</sup> with *AlbCre*. (A) Western blot of whole liver lysate for the expression of Bcl-xL and Bid. (B) Representative pictures of liver histology stained with hematoxylin-eosin and TUNEL. Arrows indicate typical apoptotic cells. (C) Western blot of whole liver lysate for the expression of cleaved caspase-7. Live lysates from wild-type mice 3 hours after intraperitoneal injection of 30 μg anti-Fas antibody (clone Jo2) or vehicle were included as a positive and a negative control, respectively. (D) Serum ALT levels. N = 14 mice per group. \**P* < 0.05 versus the other five groups; \*\**P* < 0.05 versus the other four groups except Bid<sup>-/-</sup> Bcl-xL<sup>-/-</sup> group. (E) Serum caspase-3/7 activity. N = 13 mice per group. \**P* < 0.05 versus the other five groups. (F) Statistics of TUNEL-positive cells. N = 6 mice per group. \* and \*\**P* < 0.05 versus all of Bcl-xL<sup>+/+</sup> groups and Bid<sup>-/-</sup> Bcl-xL<sup>-/-</sup> group.

apoptosis caused by Bcl-xL deficiency is completely dependent on the BH3-only protein Bid. Bid is activated by tumor necrosis factor (TNF) receptor,<sup>15</sup> and TNF-α, which is a ligand of TNF receptor, is produced by Myd88 signal pathway.<sup>16</sup> To examine the possibility of involvement of Myd88 or TNF-α in this apoptosis, we generated Myd88 Bcl-xL double-KO mice by crossing *myd88*<sup>-/-</sup> mice with *bcl-x*<sup>fllox/fllox</sup> *AlbCre* mice and administered neutralizing anti-TNF-α antibody into Bcl-xL KO mice. Hepatocyte apoptosis caused by Bcl-xL deficiency was not ameliorated with Myd88 KO background or by administration of anti-TNF-α antibody (Supporting Fig. 2A, B).

**Hepatocyte Apoptosis Caused by Bcl-xL Deficiency Requires Both Bak and Bax.** To depict the precise relationships among core Bcl-2 family proteins in regulating liver homeostasis, hepatocyte-specific Bcl-xL-deficient mice were crossed with traditional Bak or Bax KO

mice. The levels of serum ALT were slightly decreased with a Bak KO background (*bak*<sup>-/-</sup> *bcl-x*<sup>fllox/fllox</sup> *AlbCre*), whereas they did not change with a Bax KO background (*bax*<sup>-/-</sup> *bcl-x*<sup>fllox/fllox</sup> *AlbCre*) (Fig. 2A, B). To examine the contribution of both Bax and Bak, Bcl-xL KO mice were crossed with conditional Bak/Bax KO mice. The levels of serum ALT were completely normalized in Bak/Bax KO background (*bak*<sup>-/-</sup> *bax*<sup>fllox/fllox</sup> *bcl-x*<sup>fllox/fllox</sup> *AlbCre*) (Fig. 2C). Hepatocyte apoptosis determined by TUNEL staining of liver sections and caspase activation determined by caspase-3/7 activity in serum also returned to background levels (Fig. 2D, E). These observations clearly indicated that apoptosis caused by Bcl-xL deficiency was generated through the Bak/Bax-dependent mitochondrial cell death pathway. To clarify the background levels of hepatocyte apoptosis, we also analyzed the liver apoptosis in *bak*<sup>-/-</sup> and *bak*<sup>-/-</sup> *bax*<sup>fllox/fllox</sup> *AlbCre* mice. Similarly, in *bid*<sup>-/-</sup>